

# Quantification and Inference of Asymmetric Relations Under Generative Exposure Mapping Models

**Soumik Purkayastha**

*Department of Biostatistics and Health Data Science  
University of Pittsburgh  
Pittsburgh, PA 15261, USA*

SOUMIK@PITT.EDU

**Peter X.-K. Song**

*Department of Biostatistics  
University of Michigan  
Ann Arbor, MI 48103, USA*

PXSONG@UMICH.EDU

**Editor:** My editor

## Abstract

In many practical studies, learning directionality between a pair of variables is of great interest while notoriously hard, especially for mechanistic relationships. This paper presents a method that examines directionality in exposure-outcome pairs when *a priori* assumptions about their relative ordering are unavailable. We propose a *coefficient of asymmetry* to quantify directional asymmetry using Shannon's entropy and propose a statistical estimation and inference framework for said estimand. Large-sample theoretical guarantees are established through data-splitting and cross-fitting techniques. The proposed methodology is extended to allow both *measured confounders* and *contamination in outcome measurements*. The methodology is extensively evaluated through extensive simulation studies, a benchmark dataset, and a real data application.

**Keywords:** cross-fitting, data-splitting, differential entropy, directionality, virtual experiment

## 1 Introduction

In many statistical applications, *ordering* among variables is prefixed according to a certain scientific hypothesis, scientific knowledge, or a problem of interest. However, when the ordering itself is of scientific interest or if statistical analyses are sensitive to the choice of ordering, an inevitable challenge lies in inferring a sense of order in a given set of variables. We posit that the notion of order (or *asymmetry*) if it exists, is reflective of an underlying generative mechanism that maps an exposure  $X$  to an outcome  $Y$ . This paper aims to develop statistical methods that quantify and infer asymmetry in a general setup for continuous data with or without contamination of outcomes. We term this general setup as the *generative exposure mapping (GEM)* that defines an underlying ordering. Conceptually, *GEMs* arise from experiments where a mechanistic procedure  $g$  yields an outcome  $Y$  for a given input exposure  $X$  through a population-level mapping  $Y = g(X)$ . Such mappings are typically governed by the outcome-generating process  $g$  along with a designated distribution  $f_X$  for the randomness of the exposure variable  $X$ . In practice, the true form of a

*GEM* may be unknown, or a hypothesized *GEM* may be invalid when the induced ordering is false. An effective strategy for the assessment of asymmetry is to prove or disprove the ordering induced from a hypothesized *GEM* through a certain statistical analytic. In this paper, we propose a conceptually easy and computationally manageable methodology based on Shannon’s information theory to quantify and inference for relational asymmetry. As evidenced in the paper, the utility of Shannon’s analytics allows us to study asymmetry with no need of estimating the mapping function  $g$ .

In exposure mapping literature, the exposure takes typically a discrete treatment (Leung, 2022) with, *say*, an equal probability of treatment allocation. In this case, all possible exposure types may be sampled into a dataset for analysis, which is arguably impossible for continuous exposure, leading to some unique features and technical difficulty in sampling and statistical analysis of asymmetry in this paper. For continuous exposures, analogously, the uniform distribution depicts a neutral, unbiased allocation of exposure in the outcome generation mechanism. This is different from Neyman-Rubin’s causal model (Rubin, 1974) which has gained great popularity in the study of causal relations in different settings (Pearl, 2009; Imbens and Rubin, 2015). Broadly, exposure mappings have conventionally been used to evaluate the impact of complex, non-linear exposure effects on an outcome of interest (Sävje et al., 2021; Leung, 2022). In the absence of errors on outcomes, according to Gao and Ding (2023), *GEM*s no longer impose a statistical model on outcomes and other sources of external randomness, and thus greatly relax the two unverifiable conditions that are key to drawing valid causal inference in Neyman-Rubin causal models, namely the Stable Unit Treatment Value Assumption (*SUTVA*) and the random assignment assumption (Imbens and Rubin, 2015). Consequently, a *GEM*-based model is deemed as a weaker, and perhaps imperfect, causal relation in comparison to Neyman-Rubin’s causal model. As a byproduct, our proposed methodology may provide a new approach to quantify and infer manifestation of the Neyman-Rubin’s causality with minimal conditions using Shannon’s entropy analytic.

The simplest occasions of asymmetry involve placing spatial or temporal ordering conditions between the two (Cox, 1992). Establishing a presumed causal ordering of variables often requires using specific subject-matter knowledge in connection to external or *a priori* information (Cox, 1990). Alternatively, distributional asymmetries are studied by factorizing the joint density  $f_{XY}$  as the product of the marginal  $f_X$  and the conditional  $f_{Y|X}$ ; see Choi et al. (2020); Tagasovska et al. (2020); Ni (2022), among others. Recently, some asymmetric measures of association have been proposed, including the generalized measure of correlation (Zheng et al., 2012) and a rank-based asymmetry measure (Chatterjee, 2020), but none has a meaningful connection to causality and directionality implied by *GEM*s. For example, in Zheng et al. (2012) the authors propose generalized measures of correlation for asymmetry and nonlinearity but they cannot track directionality implied by *GEM*s. Similarly, Chatterjee (2020) proposes a rank-based measure of association that is asymmetric, but fails to reflect any generative mechanism. Moreover, the measures proposed fail to capture directionality when  $(X, Y)$  are linked by a bijective mapping  $Y = g(X)$ .

The role of ordering in causal inference is apparent where the existence of *a priori* direction of causation is inherently hypothesized. This prompts the need for *causal discovery* on learning underlying causal structures from observational data (Pearl, 2009). Unfortunately, this direction is not always known beforehand, especially in observational studies. A motivating epigenetic study in this paper revolves around directionality in the observed

association (Hong et al., 2023) between *DNA* methylation and blood pressure. Investigating such directionality, or asymmetry, presents a critical supplement in causal inference studies. Hence, asymmetry may be deemed as a low-level manifestation of underlying causality.

Our primary goal is to utilize a *GEM* framework to capture pairwise distributional (or population-level) *asymmetries*. This framework is based on an exposure mapping  $g$  that maps an exposure  $X$  governed by a distribution in a designed experiment to outcome  $Y$ . This function  $g$  is called a *generative function* that gives rise to a *coefficient of asymmetry* reflective of the underlying asymmetry between  $X$  and  $Y$ . Thus, proving or disproving the asymmetry implied by the hypothesized *GEM* leads to a discovery of asymmetry.

We establish a self-contained theoretical framework that significantly broadens the existing information geometric principles (Daniušis et al., 2010; Janzing et al., 2012) for examining asymmetry in exposure-outcome pairs with a new addition of statistical inference to quantify the uncertainty in the determination of underlying directionality. We organize the paper as follows: Section 2 introduces the setup of *GEMs* and some basic information theoretic concepts. Section 3 concerns a population-level measure of asymmetry under a hypothesized *GEM*, whose connection to the causal discovery framework named *information geometric causal inference (IGCI)* (Janzing et al., 2012) is discussed. Section 4 extends the population-level *GEMs* to allow for errors in the outcome  $Y$  with technical justifications for both feasibility and robustness of the proposed coefficient of asymmetry with random samples from the *GEM*. Section 6 discusses an important extension by allowing confounders in *GEMs*. Section 7 presents estimation and inference details; we implement a fast Fourier transformation-based density estimation technique to estimate key estimands of interest under a null *GEM*, followed by a cross-fitting technique to quantify estimation uncertainty while improving statistical efficiency. Finally, Sections 8 and 9 exhibit the performance of the proposed framework, estimation, and inference through simulation studies and real data applications respectively.

## 2 Preliminaries

We begin by outlining basic concepts and notation used throughout our paper. We first define the settings of our *GEM* and then introduce some elementary information theoretic concepts that are key to our framework.

### 2.1 The generative exposure mapping setup

Let us consider a population  $\mathcal{U}$  of units indexed by  $i = 1, \dots, n$  on which a randomized experiment is performed. Since an experimental design details the selection of a particular exposure value  $x$  from the support  $\mathcal{X}$  of continuous exposure  $X$ , we can say the probability density function (PDF) of  $X$ , given by  $f_X$ , governs the experiment. Let the  $i$ -th population unit independently get exposure  $X_i$ .

According to Cox (1990, 1992), a causal link between  $X$  and outcome  $Y$  must be explained through (i) a mechanism governing the exposure and (ii) a generative process yielding the outcome, with exposure as the input. We consider a structured generative mechanism specified by the *GEM* of the form with a null ordering between two variables:

$$Y = g(X), \tag{1}$$

where  $X$  is the exposure, governed by a density function  $f_X$ , and  $g$  is the unknown underlying generative function (GF) that yields the continuous outcome  $Y$ . Let  $Y_i = g(X_i)$  be the outcome of the  $i$ -th population unit in  $\mathcal{U}$ , which are assumed to be independent. Note that randomness in  $Y$ , described by its PDF  $f_Y$ , is dictated entirely by  $f_X$  and  $g$ . The exposure mapping model of [Aronow and Samii \(2017\)](#) is noted to be a special case of the *GEM* in (1) for discrete  $X$  and is further equivalent to the “effective treatments” setup described by [Manski \(2013\)](#). The overall challenges of examining asymmetry in *GEMs* involve inferring whether exposure  $X$  yields outcome  $Y$  from paired observations  $\{(x_i, y_i)\}_{i=1}^n$  or *vice-versa*. We focus exclusively assessing asymmetry in *GEMs* by leveraging information-theoretic notions of *mutual information (MI)* and *entropy*. To ensure our method is agnostic to the underlying scale of either  $X$  or  $Y$ , in this paper both variables are assumed to be invariant for both location shift and scaling transformations. Otherwise, we simply normalize the data by considering the following affine transformation given by  $(x_i - \min(x_i)) / (\max(x_i) - \min(x_i))$  for exposure  $X$  and the same operation for outcome  $Y$ . The subsequent section provides a brief review of *MI* and entropy, which will play key roles in quantifying asymmetry in *GEMs*.

## 2.2 Basic information theoretic concepts

Let  $X$  and  $Y$  be two random variables with joint density function  $f_{XY}$ . Let  $f_X$  and  $f_Y$  be the marginal densities of  $X$  and  $Y$ , respectively. Further, let  $\mathcal{X}$  and  $\mathcal{Y}$  denote the respective support sets of  $X$  and  $Y$ . Then, *mutual information* of  $X$  and  $Y$  ([Shannon, 1948](#)) is  $MI(X, Y) = E_{XY} \{\log [f_{XY}(X, Y) / \{f_X(X)f_Y(Y)\}]\}$ . The *joint differential entropy* of  $(X, Y)$  and *marginal differential entropy* of  $X$  are given by  $H(X, Y) = E_{XY} \{-\log f_{XY}(X, Y)\}$  and  $H(X) = E_X \{-\log f_X(X)\}$  respectively. Differential entropy measures the randomness of a continuous random variable ([Orlitsky, 2003](#)) and is a limiting case of Shannon’s entropy, which was originally described for discrete random variables. For the remainder of this paper, we omit the word differential, although our focus is always continuous random variables. We define the *conditional entropy function* of  $Y | X = x$  as  $H(Y | X = x) = \int_{y \in \mathcal{Y}} -\log (f_{Y|x}(y|x)) f_{Y|x}(y|x) dy$ , where  $f_{Y|x}$  denotes the conditional distribution of  $Y | X = x$ . Moreover, we have the aggregated *conditional entropy*  $H(Y | X) = \int_{x \in \mathcal{X}} H(Y | X = x) f_X(x) dx$ , which is related to the marginal and joint entropy terms through the chain rule  $H(X, Y) = H(Y | X) + H(X) = H(X | Y) + H(Y)$ . The identity may be interpreted as saying that uncertainty about  $X$  and  $Y$  may be decomposed into marginal uncertainty about  $X$  and conditional uncertainty about  $Y$ , given  $X$ ; an equivalent statement holds for marginal uncertainty regarding  $Y$  and conditional uncertainty regarding  $X$ , given  $Y$ . In the next section, we demonstrate the flexibility and capacity of Shannon’s entropy measure to quantify asymmetry under *GEMs*. Since said asymmetry is induced from a generative model, it is termed as *strong asymmetry* in this context with a certain generation process linking exposure and outcome.

## 3 Strong asymmetry in *GEMs*

In this section we derive a legitimate population-level measure of ordering or asymmetry under a hypothesized *GEM*, which is the estimand useful for the building of a statistical

procedure approving or disapproving the induced ordering from the null *GEM*. Methods that examine asymmetry typically consider non-invertible GFs (Friedman and Nachman, 2000) with added noise (Hoyer et al., 2008) only. In this section, we adopt the *IGCI* approach to showcase the ability of Shannon’s entropy to capture the strong asymmetry generated by a hypothesized *GEM* model.

### 3.1 Information geometric causal inference (*IGCI*)

Let us begin with the case of a *GEM* as described by (1); intuitively, we consider the exposure  $X$  is collected from an experiment that is governed by a density  $f_X$ . This setup is often used in Fisher’s fiducial inference (Hannig et al., 2016) in which errors, although unobservable in practice, may be simulated from a certain pivotal distribution. With  $X$  serving as an input, the *GF*  $g$  generates the population-level outcome  $Y = g(X)$ , which has density  $f_Y$ . Note that  $f_Y$  is affected both by the law governing the experiment  $f_X$  and the *GF*  $g$ . We assume  $g$  is a continuous nonlinear bijective *GF* with its inverse function given by  $g^{-1}$ , which may be used to prove or disprove the ordering induced by the reverse *GEM* given by  $X = g^{-1}(Y)$ . We rule out the case of linear  $g$  as non-informative in our setting, as it is not possible to identify the underlying direction in the *GEM* with linear  $g$  (Daniušis et al., 2010). Later, we will extend this setting to a *GEM* with added noise, which we term as the noise-perturbed *GEM*, or *NPGEM*. To begin with, let  $X$  and  $Y$  be properly scaled and are distributed on compact support  $\mathcal{X}$ , although this assumption will be relaxed to cases where  $X$  and  $Y$  do not have compact support.

An identifiability assumption required to unearth the induced asymmetry from a *GEM* is that the distribution of exposure  $X$  (or the law of  $X$ ) and the mechanism of the *GF*  $g$  do not influence each other when yielding the outcome  $Y$ , which we quantify through functional orthogonality. In the literature of functional analysis, orthogonality is appropriate to characterize the notion of “no influence”, which will be adopted in this paper.

**Assumption 1.** *Let  $g$  be a continuous nonlinear bijective function and  $f_X$  be the density that governs an experiment with exposure  $X$  with compact support  $\mathcal{X}$  that satisfies  $\int_{\mathcal{X}} \log(|\nabla g(x)|) f_X(x) dx = \int_{\mathcal{X}} \log(|\nabla g(x)|) dx$ , where the  $\nabla$  operator denotes the gradient of  $g$  with respect to its argument.*

**Remark 1.** *Assumption 1 automatically holds when  $X \sim \mathcal{U}(0,1)$ . This is analogous to the assumption of randomization or no confounding in the school of Neyman-Rubin causality, while the uniform distribution on  $X$  is analogous to randomization in an experiment that leads to no bias in operating exposure  $X$ .*

The insight in Remark 1 is key to linking the statistical understanding of randomization to information theory, where randomization may be quantified using entropy. The higher the entropy, the more random the data-generating process such as the allocation of exposure variable  $X$ . In that sense, the uniform distribution is maximally random because no distribution  $f_X$  on compact support  $\mathcal{X}$  can have greater entropy than the uniform on the same support (Cover, 2005). This maximal entropy effectively characterizes a randomized experiment with no bias in the manipulation of exposure  $X$ . To embed Assumption 1 in Shannon’s information-theoretic context, we introduce a “pseudo-variable” arising out of a “virtual randomized experiment” governed by the uniform distribution  $u_X$  on the support

of  $X$  to serve as the randomized version of exposure  $X$ . Similarly, we introduce a pseudo-variable with a uniform distribution  $u_Y$  to serve as the randomized version of outcome  $Y$ , which occurs in the absence of an exposure  $X$  in the system. Using this notation, we place Assumption 1 in the context of such virtual experiments as follows.

**Remark 2.** *Let  $g$  be a continuous nonlinear bijective GF with a differentiable inverse  $g^{-1}$  in GEM given by  $Y = g(X)$ . Let  $f_X$  be the density of the exposure  $X$  with a pseudo-variable having a uniform density  $u_X$ . Similarly, let  $f_Y$  be the density of the outcome  $Y$  with a pseudo-variable having a uniform density  $u_Y$ . Under the same GEM, the pseudo-variable with input density  $u_X$  yields an output density  $u_g(y) := |\nabla g^{-1}(y)|$ . Under the reversed GEM model  $X = g^{-1}(Y)$ , the pseudo-variable with input density  $u_Y$  yields an output density  $u_{g^{-1}}(x) := |\nabla g(x)|$ . We assume that the equality  $\int_{\mathcal{X}} f_X(x) \log\left(\frac{u_{g^{-1}}(x)}{u_X(x)}\right) dx = \int_{\mathcal{X}} u_X(x) \log\left(\frac{u_{g^{-1}}(x)}{u_X(x)}\right) dx$  holds, where the ratio  $u_{g^{-1}}(x)/u_X(x)$  characterizes the contrast of likelihood that the exposure is generated from the underlying inverse generative model with the outcome as input, rather than from a randomized virtual experiment.*

**Remark 3.** *Similar to counterfactual-based causality, when the randomization is lost, covariate adjustment is a commonly used approach to mitigate or remove bias in the sampling of exposure. The stratification principle advocated by Fisher (1925) has been broadly used in practice. Technically, we may confounders  $\mathbf{Z}$  in the GEM, leading to an extended Assumption 1:  $\int_{\mathcal{X}} \log(|\nabla_X g(x, \mathbf{z})|) f_X(x|\mathbf{z}) dx = \int_{\mathcal{X}} \log(|\nabla_X g(x, \mathbf{z})|) dx$ , where  $Y = g(X, \mathbf{Z})$  is an extended GEM and  $\nabla_X g(x, \mathbf{z})$  denotes the partial derivative of the GF  $g$  with respect to  $X$  when  $\mathbf{Z} = \mathbf{z}$  is fixed. This implies that if  $f_X(x|\mathbf{z})$  is uniformly distributed, then the generative mapping is preserved under the conditional distribution.*

### 3.2 Asymmetry in GEMs for uniformly distributed exposure $X$

The following Lemma 1 from Daniušis et al. (2010) declares the emerging of a population-level asymmetry under a GEM when the exposure is uniformly distributed, which mirrors an underlying exposure that is “balanced” with no bias and near-perfect randomization.

**Lemma 1.** *Assume that a zero-noise GEM given by  $Y = g(X)$  satisfies Assumption 1, where the GF  $g$  is a continuous nonlinear bijective function with differentiable inverse  $g^{-1}$  with uniformly distributed exposure  $X$ . Then, the density  $f_Y$  of the generated outcome  $Y$   $\int \log(|\nabla g^{-1}(y)|) f_Y(y) dy \geq \int \log(|\nabla g^{-1}(y)|) dy$ , with equality if and only if  $\nabla g$  is constant or equivalently  $g$  is a linear function of  $x$ .*

Lemma 1 implies (i) in the class of linear generative models, asymmetry is void as information flows in two directions are of no difference; (ii) given a uniformly distributed exposure  $X$ , the generated outcome  $Y$  is no longer uniform, and (iii) a certain mixing occurs between the dynamics of the inverse GF and the generated outcome in the way that the former is augmented by the outcome’s non-uniform distribution. That is, the retrieval of  $X$  from  $Y$  via  $g^{-1}$  involves more dynamics, which in turn signifies asymmetry. In summary, the GEM generates outcome  $Y$  from the uniformly distributed exposure  $X$  through a smooth bijective GF  $g$ , where the distribution of outcome  $Y$  is found to be less random than the uniformly distributed exposure  $X$  that is maximally random. This discrepancy or

asymmetry in the information exchange provides a useful perspective to capture and confirm the asymmetry under a generative mechanism even when the underlying exposure is not uniformly distributed, subject to some identifiability conditions. We describe quantifying this asymmetry in Section 3.3 using Shannon’s entropy analytic.

### 3.3 Entropy-based quantification of induced asymmetry

When Assumption 1 holds, Lemma 1 establishes an induced asymmetry from uniformly distributed exposure  $X$  to outcome  $Y$  that is generated by a  $GEM$ . However, when  $X$  is not uniformly distributed, we may embed Assumption 1 in the setting of pseudo-variables with underlying uniform densities as described in Remark 2. It is worth noting that Remark 2 gives rise to a kind of orthogonality that may be expressed using Kullback-Leibler divergences (Cover, 2005). Moreover, the following information-theoretic Pythagorean theorem allows us to establish strong asymmetry under a  $GEM$  with an exposure  $X$  being no longer uniformly distributed.

We consider three generic probability densities  $p, q$ , and  $r$  defined over support  $\mathcal{X}$ . Let  $KL(p \parallel q)$  denote the Kullback-Leibler divergence between two densities, say,  $p$  and  $q$ , which is defined by  $KL(p \parallel q) = \int_{\mathcal{X}} p(x) \log \left( \frac{p(x)}{q(x)} \right) dx$ . It is easy to show that the Pythagorean identity  $KL(p \parallel q) + KL(q \parallel r) = KL(p \parallel r)$ , holds under the condition given by  $\int_{\mathcal{X}} p(x) \log \frac{q(x)}{r(x)} dx = \int_{\mathcal{X}} q(x) \log \frac{q(x)}{r(x)} dx$ . This Pythagorean relation reflects a kind of information orthogonality between the link of density pair  $(p, q)$  and the link of density pair  $(q, r)$ . We can rewrite Remark 2 and obtain a similar Pythagorean relation:  $KL(f_X \parallel u_X) + KL(u_X \parallel u_{g^{-1}}) = KL(f_X \parallel u_{g^{-1}})$ . Further, since KL divergences are preserved under bijective maps, we can write  $KL(f_X \parallel u_X) + KL(u_g \parallel u_Y) = KL(f_Y \parallel u_Y)$ . Moreover, we yield the key inequality in a general setting as follows:

$$KL(f_X \parallel u_X) \leq KL(f_Y \parallel u_Y), \tag{2}$$

which is a consequential property from the generative mechanism governed by the  $GEM$  described in Remark 2. Intuitively,  $KL(f_X \parallel u_X)$  measures the distance between the true density  $f_X$  that governs exposure  $X$  in the actual experiment versus the uniform distribution  $u_X$  that mirrors the virtual randomized experiment. Similarly,  $KL(f_Y \parallel u_Y)$  measures the distance of actual distribution  $f_Y$  from the uniform distribution  $u_Y$ . The inequality in (2) suggests that the distance of the outcome density  $f_Y$  from its corresponding uniform density  $u_Y$  is always more than the distance of the exposure density  $f_X$  from its corresponding uniform density  $u_X$ . More importantly, (2) aligns with the direction of asymmetry in  $X$  and  $Y$  under a hypothesized  $GEM$ .

Motivated by the connection between uniform distributions and randomized allocation of exposure, we may set both  $u_X$  and  $u_Y$  to be identically the uniform density (that equals to a constant  $1/|\mathcal{X}|$ ), mirroring the complete randomization of the hypothetical virtual experiment. Thus, under such virtual randomized experiment, the asymmetry via the inequality in (2) may be quantified by their difference:

$$C_{X \succ Y} := KL(f_Y \parallel u_Y) - KL(f_X \parallel u_X) = H(X) - H(Y), \tag{3}$$

where the last equality holds under both  $u_X$  and  $u_Y$  being the uniform distributions. Using the contrast in (3), we can formally define a population-level strong asymmetry below.

**Definition 1.** Let  $g$  be a continuous nonlinear bijective generative function in the GEM  $Y = g(X)$ .  $C_{X \succ Y}$  in (3) is termed as the strong asymmetry coefficient (SAC). If the equality in Remark 2 holds, the pair  $(X, Y)$  are said to be strongly asymmetric if  $C_{X \succ Y} \neq 0$ , denoted by  $X \succ_s Y$  if  $C_{X \succ Y} > 0$ , or by  $Y \succ_s X$  if  $C_{X \succ Y} < 0$ .

**Remark 4.** To deal with unbounded domain for these two variables, we may use diffused normal distributions that are approximately uniform as the hypothetical densities of the virtual experiments; in effect,  $u_X$  and  $u_Y$  are both normal distribution with mean  $\mu$  (e.g. 0) and a large variance  $\sigma_u^2$  (e.g.  $10^4$ ).

We examine the estimated coefficient of asymmetry given by  $\hat{C}_{X \succ Y} := \hat{H}(X) - \hat{H}(Y)$ , where  $\hat{H}(X)$  and  $\hat{H}(Y)$  are estimated marginal entropies of  $X$  and  $Y$  respectively. The positive sign of  $\hat{C}_{X \succ Y}$  approves the induced ordering given in the GEM  $Y = g(X)$  where hypothetically  $X$  produces  $Y$ ; otherwise, the opposite directionality is declared. In practice it is possible to encounter a third case with  $\hat{H}(X) \approx \hat{H}(Y)$ , namely neither direction is suggested by data at hands, implying a symmetric relation.

#### 4 Strong asymmetry with noise perturbation

In a practical data generation scenario, measurement errors or noise perturbations are inevitable. Thus, we now extend the setup of the previously noise-free GEM by adding randomness on the outcome  $Y$ , so a noise-perturbed GEM (NPGEM) takes the form:

$$Y^* = g(X) + \epsilon, \text{ such that } \epsilon \perp X, \text{ and } \mathbb{E}(\epsilon) = 0, \mathbb{V}(\epsilon) = \sigma, \quad (4)$$

where  $Y^*$  is the ‘‘contaminated’’ version of outcome  $Y$ . Note that Manski (2013); Aronow and Samii (2017) describe exposure mappings only in the context of discrete exposures and do not allow for any other source of randomness in the generative mechanism linking exposure to outcome (i.e.  $\sigma = 0$ ). In their GEMs, randomness in outcome  $Y$  is attributed exclusively to either (i) randomness in exposure  $X$  or (ii) the dynamics of the GF  $g$ . In contrast, the GEMs as well as statistical methods considered in this paper are extended to accommodate continuous variables with added noise on outcome measurements. From Definition 1, note that the SAC can measure the population-level asymmetry between exposure and outcome even with noise perturbation when we encounter  $Y^*$  instead of  $Y$  in the population-level model, so long as the ordering of  $H(Y^*)$  being lower than  $H(X)$  is preserved. We now justify the validity of SAC in NPGEMs with the variance of the error  $\epsilon$  being capped at a level so that  $SAC > 0$  is preserved even under noise perturbation. To do so, we introduce an intermediate NPGEM with normally distributed disturbance  $Z$  having mean 0 and variance 1, such that  $H(Y^*) \leq H(Y + \sqrt{\sigma'}Z)$  for a certain  $\sigma' > 0$ . This NPGEM is merely for a technical need; de Bruijn’s theorem (Cover, 2005) has shown that  $H(Y + \sqrt{\sigma'}Z)$  is an increasing function of  $\sigma'$ . We state the following Theorem:

**Theorem 1.** In the noise-free GEM  $Y = g(X)$ , let  $f_Y$  and  $H(Y)$  denote the density and entropy of  $Y$  respectively. We consider a noise disturbance  $\epsilon$  in the NPGEM. Then, the upper-bound on the entropy of  $Y^*$  is given by  $H(Y^*) \leq H(Y) + \frac{1}{2} \log(\sigma' I(Y) + 1)$ , where  $\sigma'$  is a value such that  $H(Y^*) \leq H(Y + \sqrt{\sigma'}Z)$  with  $Z \sim N(0, 1)$  and  $X \perp Z$ , and  $I(Y) := \mathbb{E}_Y [\nabla_Y \log(f_Y(Y))]^2$  is the (nonparametric) Fisher information of  $Y$ .



Note that the existence of the  $\sigma'$  is ensured by de Bruijn's identity. We refer the reader to the appendix for the proof of Theorem 1. To ensure the *SAC* properly measures the induced asymmetry in an *NPGEM* with no influence from the noise perturbation, we must have  $H(Y^*) \leq H(Y) + \log(\sigma' I(Y) + 1) / 2 < H(X)$ , implying

$$I(Y) < \frac{\exp(2C_{X \succ Y}) - 1}{\sigma'} = \frac{\exp(2C_{X \succ Y}) - \exp(2C_{X \succ Y}^0)}{\sigma'}, \quad (5)$$

where  $C_{X \succ Y}^0 \equiv 0$  is value of  $C_{X \succ Y}$  in a *balanced* or *symmetric* relation. We argue that the numerator  $\exp(2C_{X \succ Y}) - \exp(2C_{X \succ Y}^0)$  is a measure of the deviation from symmetry and serves as the signal that our method must capture. To arrive at (5), note that we have (i)  $C_{X \succ Y} = H(X) - H(Y) > 0$ , and (ii) Theorem 1 ensures  $\sigma' I(Y) < \exp(2C_{X \succ Y}) - \exp(2C_{X \succ Y}^0)$ . Hence, the *strong asymmetry* framework works in low-noise regimes of the *NPGEM* where (5) provides a lower bound on the signal-to-noise ratio that the *SAC* can tolerate and remains effective to quantify *NPGEM*-induced asymmetry.

**Remark 5.** In (4), if we further assume  $\epsilon \sim N(0, \sigma)$ , then we have a more refined bound than (5), given by  $I(Y) < \{\exp(2C_{X \succ Y}) - 1\} / \sigma = \{\exp(2C_{X \succ Y}) - \exp(2C_{X \succ Y}^0)\} / \sigma$ . The key difference lies in the fact that the former does not impose distributional assumptions on the contaminant  $\epsilon$ , whereas the latter requires  $\epsilon \sim N(0, \sigma)$ .

## 5 Weak asymmetry in absence of *GEMs*

We argue that *SAC* can also capture asymmetric relations where *GEMs* are absent. This is because  $H(X | Y) > H(Y | X)$  implies less uncertainty in  $Y$  after conditioning on  $X$  than the converse. That is,  $X$  exerts more influence on  $Y$  than  $Y$  does on  $X$ . It is reasonable to assume that such an unbalanced predictive capacity may be an imprint of underlying asymmetry in exposure-outcome pairs, yielding the definition of weak asymmetry.

**Definition 2.** Two random variables  $X$  and  $Y$  are said to be weakly asymmetric if their conditional entropy terms are unbalanced, denoted by  $X \succ_w Y$  if  $H(X | Y) > H(Y | X)$  or by  $Y \succ_w X$  if  $H(Y | X) > H(X | Y)$ . The weak asymmetry coefficient (*WAC*) is defined as the contrast  $H(X | Y) - H(Y | X)$ . The *WAC* can be conveniently computed from the chain rule, i.e.,  $WAC = H(X | Y) - H(Y | X) = H(X) - H(Y)$ . Thus, the difference or *WAC* can be evaluated through the marginal entropy quantities.

Definition 2 gives rise to a simple and quick approach to scrutinizing a putative asymmetric relation between exposure and outcome without imposing any hypothesized generative mechanisms. The  $C_{X \succ Y}$ -based decision rule first compares the differential entropy of  $X$  and  $Y$  and considers the variable with lower differential entropy as the outcome in our weak asymmetry framework. Violating this asymmetry may pose strong doubts about the underlying asymmetric relation between exposure and outcome.

**Remark 6.** While strong asymmetry implies weak asymmetry, the converse is not true. The sign of  $C_{X \succ Y}$  suffices inferring weak asymmetry, whereas the strong asymmetry framework requires an underlying generative mechanism specified by the *GEM* with further identifiability assumptions on the *GF*  $g$  to infer strong asymmetry based on the sign of  $C_{X \succ Y}$ .

## 6 Adjusting for confounding factors

We now discuss an extension by including confounding factors  $\mathbf{Z}$  within our generative framework. We will describe a framework to infer asymmetry in  $(X, Y)$  from observations  $\{(x_i, y_i)\}_{i=1}^n$  given observations  $\{\mathbf{z}_i\}_{i=1}^n$  on confounders  $\mathbf{Z}$ . In this paper, we will restrict ourselves to accounting for low-dimensional confounder effects. We explore two related questions: first, we propose a framework for examining asymmetry between  $(X, Y)$  given a specific value of observed confounder(s)  $\mathbf{Z} = \mathbf{z}$ ; next, we propose an extension that examines asymmetry between  $(X, Y)$  conditioned across all values in the support  $\mathcal{Z}$ . While the former approach will allow for strata-specific comparisons of asymmetry between  $(X, Y \mid \mathbf{Z} = \mathbf{z})$  given a fixed value  $\mathbf{Z} = \mathbf{z}$ , the latter will facilitate population-level comparisons of asymmetry between  $(X, Y \mid \mathbf{Z})$  for confounder(s)  $\mathbf{Z}$ . With no surprise, estimating the coefficients proposed below appears slightly more involved than the coefficient  $\hat{C}_{X \succ Y}$  without confounder(s). Let  $Y = g(X, \mathbf{Z})$  be the *GEM* under consideration and  $\nabla_X g(x, \mathbf{z})$  denotes the partial derivative of  $g$  with respect to argument  $X$  when confounder(s)  $\mathbf{Z} = \mathbf{z}$  is fixed. We further assume the equality in Remark 3 to hold for a fixed value of the confounder  $\mathbf{Z} = \mathbf{z}$ . Extending the *SAC* for *GEMs* in Section 3 to adjust for confounder(s)  $\mathbf{Z}$ , we propose the measure  $C_{X \succ Y \mid \mathbf{Z} = \mathbf{z}} = H(X \mid \mathbf{Z} = \mathbf{z}) - H(Y \mid \mathbf{Z} = \mathbf{z})$ , to serve as the measure to quantify strong asymmetry in  $(X, Y)$  for a specific value of observed confounder  $\mathbf{Z} = \mathbf{z}$ . If strong asymmetry in a specific direction holds for all values  $\mathbf{z} \in \mathcal{Z}$ , i.e., say, if  $C_{X \succ Y \mid \mathbf{Z} = \mathbf{z}} > 0$  all  $\mathbf{z} \in \mathcal{Z}$ , we can further yield an aggregated measure of strong asymmetry in  $(X, Y \mid \mathbf{Z})$ , given as follows:

$$C_{X \succ Y \mid \mathbf{Z}} = \mathbb{E}_{\mathbf{Z}} \{C_{X \succ Y \mid \mathbf{Z} = \mathbf{z}}\} = H(X \mid \mathbf{Z}) - H(Y \mid \mathbf{Z}) = H(X, \mathbf{Z}) - H(Y, \mathbf{Z}), \quad (6)$$

where the last equality follows from the chain rule. Here  $F_{\mathbf{Z}}$  is the distribution function of  $\mathbf{Z}$  defined over support  $\mathcal{Z}$ . In (6) we may assume  $\mathbf{Z}$  has a density function  $f_{\mathbf{Z}}$  defined on  $\mathcal{Z}$ , although the same approach holds for discrete  $\mathbf{Z}$  as well; i.e., we replace  $f_{\mathbf{Z}}$  with the mass function  $p_{\mathbf{Z}}$  and exchange the integration with summation operator over discrete  $\mathbf{Z} \in \mathcal{Z}$ . Further, if strong asymmetry in a specific direction holds for all values  $\mathbf{z} \in \mathcal{Z}$ , (6) yields a population-level measure of strong asymmetry in  $(X, Y \mid \mathbf{Z})$ . Finally, in absence of a *GEM* or identifiability assumption given by Remark 3, the measure given by  $C_{X \succ Y \mid \mathbf{Z} = \mathbf{z}}$  serves as a measure of weak asymmetry in  $(X, Y)$  for specified  $\mathbf{Z} = \mathbf{z}$ .

## 7 Estimation and inference

In either framework of *weak* or *strong asymmetry*, we must estimate and perform inference using  $\hat{C}_{X \succ Y}$ . To do so, we must first estimate the underlying marginal densities  $f_X$  and  $f_Y$ , which may be thought of as infinite-dimensional nuisance parameters. If the same data that were used for density estimation are also used to provide inference for  $C_{X \succ Y}$ , standard inferential procedures may suffer from bias. To circumvent this, we consider a data-splitting and cross-fitting approach (Chernozhukov et al., 2018). This technique is key to providing a stable estimator and is one of the main novelties of our method.

The density estimation technique in Section 7.1 provides an accurate and fast solution without incurring the need for tuning parameters. Considering the potential use of *SAC* to examine a large number of pairwise relations, we want to choose an computationally

efficient nonparametric density estimation method. Based on the estimated densities, we obtain consistent estimates of  $\hat{C}_{X \succ Y}$ . Next, in Section 7.2, we describe the data-splitting and cross-fitting technique that allows us to provide an inference rule for testing asymmetry in the possibly contaminated *GEM* given by  $Y^* = g(X) + \epsilon$ .

### 7.1 Self-consistent density estimation

The self-consistent estimator (SCE) was proposed by [Bernacchia and Pigolotti \(2011\)](#); [O’Brien et al. \(2016\)](#) to minimize the mean integrated squared error (MISE) between the estimated density and the true density without incurring any manual parameter tuning. The estimation process relies on fast Fourier transforms (FFT). Utilizing this ‘optimal’ density estimator, [Purkayastha and Song \(2023\)](#) propose a plug-in estimator of *MI*, termed as the **fastMI**, which is shown to be a consistent and fast estimator. Extending the usage of the self-consistent density estimator here, we then estimate the marginal entropies  $\hat{H}(X)$  and  $\hat{H}(Y)$ , thereby obtaining an estimate of  $\hat{C}_{X \succ Y}$ .

Let us consider a random sample denoted by  $\mathcal{S} = \{X_1, X_2, \dots, X_n\}$  from an unknown density  $f$  with support  $\mathcal{X}$  (without loss of generality,  $\mathcal{X} = \mathbb{R}$ ). We assume  $f$  belongs to the Hilbert space of square-integrable functions, given by  $\mathcal{L}^2 = \{f : \int f^2(x)dx < \infty\}$ . The SCE is denoted by  $\hat{f} \in \mathcal{L}^2$ . First, in order to define  $\hat{f}$ , we require a kernel function  $\mathcal{K}$ , which belongs to the class of functions given by  $\mathbb{K} := \{\mathcal{K} : \mathcal{K}(x) \geq 0, \mathcal{K}(x) = \mathcal{K}(-x); \int \mathcal{K}(t)dt = 1\}$ . Specifically,  $\hat{f}$  is the convolution of a kernel  $\mathcal{K}$  and delta functions centered on the dataset:

$$\hat{f}(z) \equiv n^{-1} \sum_{j=1}^n \mathcal{K}(x - X_j) = n^{-1} \sum_{j=1}^n \int_{\mathbb{R}} \mathcal{K}(s) \delta(x - X_j - s) ds, \quad x \in \mathbb{R} \quad (7)$$

where  $\delta(x)$  is the Dirac delta function. The optimal  $\hat{f}$  is identified by the optimal kernel  $\hat{\mathcal{K}}$ , where ‘optimality’ is intended as minimising the mean integrated square error (*MISE*) between the true density  $f$  and the estimator  $\hat{f}$ :

$$\hat{\mathcal{K}} = \operatorname{argmin}_{\mathcal{K} \in \mathbb{K}} \operatorname{MISE}(\hat{f}, f) = \operatorname{argmin}_{\mathcal{K} \in \mathbb{K}} \mathbb{E} \left[ \int_{\mathbb{R}} \{\hat{f}(x) - f(x)\}^2 dx \right], \quad (8)$$

where the  $\mathbb{E}$  operator denotes taking expectation over the entire support of  $f$ . The SCE in (7) may be represented equivalently by its inverse Fourier transform pair,  $\hat{\phi} \in \mathcal{L}^2$ , given by  $\hat{\phi}(t) = \mathcal{F}^{-1}(\hat{f}(z)) = \kappa(t)\mathcal{C}(t)$ , where  $\mathcal{F}^{-1}$  represents the multidimensional inverse Fourier transformation from space of data  $z \in \mathbb{R}$  to frequency space coordinates  $t \in \mathbb{R}$ .  $\kappa = \mathcal{F}^{-1}(\mathcal{K})$  is the inverse Fourier transform of the kernel  $\mathcal{K}$  and  $\mathcal{C}$  is the empirical characteristic function (ECF) of the data, defined as  $\mathcal{C}(t) = n^{-1} \sum_{j=1}^n \exp(itZ_j)$ . [Bernacchia and Pigolotti \(2011\)](#) derive the optimal transform kernel  $\hat{\kappa}$  minimizing the *MISE* given by (8), given as follows:

$$\hat{\kappa}(t) = \frac{n}{2(n-1)} \left[ 1 + \sqrt{1 - \frac{4(n-1)}{|n\mathcal{C}(t)|^2}} \right] I_{A_n}(t), \quad (9)$$

where  $A_n$  serves as a low-pass filter that yields a stable estimator ([Purkayastha and Song, 2023](#)). We follow the nomenclature of [Bernacchia and Pigolotti \(2011\)](#) and denote  $A_n$  as the set of ‘acceptable frequencies’. The optimal transform kernel  $\hat{\kappa}$  in (9) may be anti-transformed back to the real space to obtain the optimal kernel  $\hat{\mathcal{K}} \in \mathbb{K}$ , which yields the

optimal density estimator  $\hat{f}$  according to Equation 7. Theorem 2 presents the sufficient conditions for the estimate  $\hat{f}$  to converge to the true density  $f$  for  $n \rightarrow \infty$ . First, we state the technical assumptions needed for Theorem 2 to hold.

**Assumption 2.** *Let the true density  $f$  be square-integrable and its corresponding Fourier transform  $\phi$  be integrable.*

**Assumption 3.** *Let us assume the following about the low-pass filter  $A_n$ :  $\mathcal{V}(A_n) \rightarrow \infty$ ,  $\mathcal{V}(A_n)/\sqrt{n} \rightarrow 0$  and  $\mathcal{V}(\bar{A}_n) \rightarrow 0$  as  $n \rightarrow \infty$ , where  $\bar{A}_n$  is the complement of  $A_n$  and the volume of  $A_n$  is given by  $\mathcal{V}(A_n)$ .*

**Assumption 4.** *Let the true density  $f$  be continuous on dense support  $\mathcal{X}$ .*

**Theorem 2.** *If Assumptions 2 and 3 hold, then the self consistent estimator  $\hat{f}$ , which is defined by (7) - (9), converges almost surely to the true density as  $n \rightarrow \infty$ . Further, if Assumption 4 holds, we have uniform almost sure convergence of  $\hat{f}$  to  $f$  as  $n \rightarrow \infty$ .*

The proof of Theorem 2 is omitted here; see Purkayastha and Song (2023) for the detail.

## 7.2 Data-splitting and cross-fitting inference

We have noted earlier that if the same data that were used for density estimation are also used to provide inference for  $C_{X \succ Y}$ , standard inferential procedures may suffer from bias (Chernozhukov et al., 2018). Here, we describe a data-splitting and cross-fitting technique to help us circumvent this issue and provide valid inference on  $\hat{C}_{X \succ Y}$ , thereby filling a gap in literature (Daniušis et al., 2010).

Let  $\mathcal{D} = \{(X_1, Y_1), \dots, (X_{2n}, Y_{2n})\}$  be a random sample drawn from a bivariate distribution  $f_{XY}$  with marginal  $f_X$  for  $X$  and  $f_Y$  for  $Y$ . Since we do not have knowledge of  $f_X$  or  $f_Y$ , we invoke a data-splitting and cross-fitting technique to estimate the underlying density functions as well as the relevant entropy terms. That is, we first split the available data  $\mathcal{D}$  into two equal-sized but disjoint sets denoted by  $\mathcal{D}_1 := \{(X_1, Y_1), \dots, (X_n, Y_n)\}$ , and  $\mathcal{D}_2 := \{(X_{n+1}, Y_{n+1}), \dots, (X_{2n}, Y_{2n})\}$ . Using one data split  $\mathcal{D}_1$ , we obtain estimates of the marginal density functions  $\hat{f}_{X;1}$  and  $\hat{f}_{Y;1}$  by the SCE method described in Section 7.1. The estimated density functions are evaluated for data belonging to the second data split  $\mathcal{D}_2$  to obtain the following estimates of marginal entropies  $\widehat{H}_2(X) = -n^{-1} \sum_{j=1}^n \ln(\hat{f}_{X;1}(X_{n+j}))$  and  $\widehat{H}_2(Y) = -n^{-1} \sum_{j=1}^n \ln(\hat{f}_{Y;1}(Y_{n+j}))$ . Interchanging the roles of data splits  $\mathcal{D}_1$  and  $\mathcal{D}_2$ , by a similar procedure, we obtain the estimated densities  $\hat{f}_{X;2}$  and  $\hat{f}_{Y;2}$ . The estimated density functions are evaluated for data belonging to data split  $\mathcal{D}_1$  to obtain the estimated entropies  $\widehat{H}_1(X) = -n^{-1} \sum_{j=1}^n \ln(\hat{f}_{X;2}(X_j))$  and  $\widehat{H}_1(Y) = -n^{-1} \sum_{j=1}^n \ln(\hat{f}_{Y;2}(Y_j))$ . Taking an average of the two sets of estimates, we obtain the so-called ‘‘cross-fitted’’ estimates of the marginal entropies  $\hat{H}(X) = \{\widehat{H}_1(X) + \widehat{H}_2(X)\} / 2$  and  $\hat{H}(Y) = \{\widehat{H}_1(Y) + \widehat{H}_2(Y)\} / 2$ . Next, we define oracle estimators of  $H_X$ , and  $H_Y$  for each of the data splits:

$$H_{0;1}(X) = -\frac{1}{n} \sum_{j=1}^n \ln(f_X(X_j)), \text{ and } H_{0;2}(X) = -\frac{1}{n} \sum_{j=1}^n \ln(f_X(X_{n+j})), \quad (10)$$

with respect to  $\mathcal{D}_1$  and

$$H_{0;1}(Y) = -\frac{1}{n} \sum_{j=1}^n \ln(f_Y(Y_j)), \text{ and } H_{0;2}(Y) = -\frac{1}{n} \sum_{j=1}^n \ln(f_Y(Y_{n+j})), \quad (11)$$

with respect to  $\mathcal{D}_2$ . The quantities so obtained are averaged to obtain the ‘‘cross-fitted oracle estimates’’ given by  $H_0(X) = \{H_{0;1}(X) + H_{0;2}(X)\} / 2$ ,  $H_0(Y) = \{H_{0;1}(Y) + H_{0;2}(Y)\} / 2$ . The following two theorems establish both consistency and asymptotic normality of the cross-fitted estimates. In addition to Assumptions 2 – 4, we impose the following assumption that is needed for Theorems 3 and 4 to hold.

**Assumption 5.** *Let the density  $f$  be bounded away from zero and infinity on its support.*

**Theorem 3.** *Let Assumptions 2 – 5 hold when estimating  $\hat{f}_X$  or  $\hat{f}_Y$  using data splits  $\mathcal{D}_1$  and  $\mathcal{D}_2$ . We implement the data-splitting and cross-fitting procedure described in Section 7.2. Then, the cross-fitted estimate is strongly consistent, i.e.,  $\hat{C}_{X \succ Y} \xrightarrow{a.s.} C_{X \succ Y}$  as  $n \rightarrow \infty$ .*

**Theorem 4.** *Let Assumptions 2 – 5 hold when estimating  $\hat{f}_X$  or  $\hat{f}_Y$  using data splits  $\mathcal{D}_1$  and  $\mathcal{D}_2$ . We implement the data-splitting procedure described in Section 7.2 to obtain cross-fitted estimates  $\hat{H}(X)$  and  $\hat{H}(Y)$  using  $\mathcal{D}_1$  and  $\mathcal{D}_2$ . Then, we have the following:*

$$\sqrt{n} \begin{pmatrix} \hat{H}(X) - H_0(X) \\ \hat{H}(Y) - H_0(Y) \end{pmatrix} \xrightarrow{\mathcal{P}} 0, \text{ as } n \rightarrow \infty. \quad (12)$$

We refer the reader to the appendix for proofs of Theorem 3 and Theorem 4.

**Lemma 2.** *By the multivariate central limit theorem, assuming  $\mathbb{V}[\log(f_X(X))] < \infty$  and  $\mathbb{V}[\log(f_Y(Y))] < \infty$ , we have  $(H_0(X), H_0(Y))'$  jointly converge in distribution, given by*

$$\sqrt{n} \begin{pmatrix} H_0(X) - H(X) \\ H_0(Y) - H(Y) \end{pmatrix} \xrightarrow{\mathcal{D}} N(\mathbf{0}, \Sigma), \text{ as } n \rightarrow \infty,$$

where  $\Sigma$  is the  $2 \times 2$  dispersion matrix of  $(H_0(X), H_0(Y))'$ .

Using Theorem 4 and Lemma 2, we get the following corollary.

**Corollary 1.** *Let Assumptions 2 – 5 hold when obtaining  $\hat{C}_{X \succ Y}$  using cross-fitted estimates from data splits  $\mathcal{D}_1$  and  $\mathcal{D}_2$ . We make use of Lemma 2 to note that  $\sqrt{n} (\hat{C}_{X \succ Y} - C_{X \succ Y}) \xrightarrow{\mathcal{D}} N(0, \sigma_C^2)$ , as  $n \rightarrow \infty$ , where  $\sigma_C^2$  denotes the asymptotic variance of the estimate  $\hat{C}_{X \succ Y}$  and can be estimated by the Monte Carlo technique, given density estimates  $\hat{f}_X$  and  $\hat{f}_Y$ .*

We refer the reader to the appendix for the proof of Corollary 1. See the appendix on how to estimate  $\hat{\sigma}_C^2$  using data-splitting and cross-fitting (Chernozhukov et al., 2018).

### 7.3 Testing for asymmetry in $GEM$ s using $C_{X \succ Y}$

The sign of  $C_{X \succ Y}$  suggests an asymmetric relation between  $X$  and  $Y$ . The one-sided null hypothesis  $H_0 : C_{X \succ Y} > 0$  postulates a putative directionality from  $X$  to  $Y$  under the  $GEM$  of  $Y = g(X)$ . This null is “protected” with a high (*say*, 95%) confidence and will be rejected if there lacks evidence that the statistic  $\hat{C}_{X \succ Y}$  is significantly bigger than zero. The asymptotic normality established in Corollary 1 is the theoretical basis for the proposed hypothesis testing method based on  $\hat{C}_{X \succ Y} = \hat{H}(X) - \hat{H}(Y)$ . That is, we construct a one-sided 95% asymptotic confidence interval (CI) of  $\hat{C}_{X \succ Y}$ , denoted by  $(\hat{L}, \infty)$  where  $\hat{L}$  is the estimated lower bound. Consequently, if zero falls outside the interval  $(\hat{L}, \infty)$  or  $\hat{L} \leq 0$ , we would reject the null hypothesis and conclude that the postulated directionality is disproved by the data at hand. Moreover, rejecting the null above implies either symmetry or reversed asymmetry. Thus, we may further consider testing the opposite directionality under an inverse  $GEM$ :  $X = g^{-1}(Y)$  by the means of confidence interval via  $\hat{C}_{Y \succ X}$ .

### 7.4 Estimating $C_{X \succ Y | \mathbf{Z} = \mathbf{z}}$ and $C_{X \succ Y | \mathbf{Z}}$ for low dimensional $\mathbf{Z}$

To estimate  $C_{X \succ Y | \mathbf{Z} = \mathbf{z}}$  we need to estimate  $H(X | \mathbf{Z} = \mathbf{z})$  as well as  $H(Y | \mathbf{Z} = \mathbf{z})$ , where  $H(X | \mathbf{Z} = \mathbf{z}) = \int_{x \in \mathcal{X}} -\log(f_{X|\mathbf{z}}(x)) f_{X|\mathbf{z}}(x) dx$ . We consider the estimate  $\hat{H}(X | \mathbf{Z} = \mathbf{z}) = \int_{x \in \mathcal{X}} -\log(\hat{f}_{X|\mathbf{z}}(x)) \hat{f}_{X|\mathbf{z}}(x) dx$ , where  $\hat{f}_{X|\mathbf{z}}$  is the estimated conditional density of  $X$  given  $\mathbf{Z} = \mathbf{z}$ . Based on whether  $\mathbf{Z}$  is discrete or continuous, we propose two separate estimation techniques. If  $\mathbf{Z}$  is discrete or categorical, for data given by  $\{x_i, y_i, \mathbf{z}_i\}_{i=1}^n$ , the estimation procedure begins by considering the following stratum of the data given by  $\mathcal{D}(\mathbf{Z} = \mathbf{z}) := \{(x_i, y_i) : \mathbf{z}_i = \mathbf{z}\}$ . Assuming a sufficiently large sample size, we may apply the data-splitting and cross-fitting technique on stratum  $\mathcal{D}(\mathbf{Z} = \mathbf{z})$ . For continuous  $\mathbf{Z}$ , our approach yields the following form of  $C_{X \succ Y | \mathbf{Z} = \mathbf{z}}$ :

$$C_{X \succ Y | \mathbf{Z} = \mathbf{z}} = \frac{1}{f_{\mathbf{Z}}(\mathbf{z})} \left\{ \int -\log(f_{X,\mathbf{z}}(x, \mathbf{z})) f_{X,\mathbf{z}}(x, \mathbf{z}) dx - \int -\log(f_{Y,\mathbf{z}}(y, \mathbf{z})) f_{Y,\mathbf{z}}(y, \mathbf{z}) dy \right\}.$$

Using **fastMI** in Section 7.1, we estimate  $\hat{f}_{X,\mathbf{z}}$ ,  $\hat{f}_{Y,\mathbf{z}}$ , and  $\hat{f}_{\mathbf{z}}$ , and obtain  $\hat{C}_{X \succ Y | \mathbf{Z} = \mathbf{z}}$  given by

$$\hat{C}_{X \succ Y | \mathbf{Z} = \mathbf{z}} = \frac{1}{\hat{f}_{\mathbf{Z}}(\mathbf{z})} \left[ \frac{1}{n} \sum_{i=1}^n -\log(\hat{f}_{X,\mathbf{z}}(X_i, \mathbf{z})) - \frac{1}{n} \sum_{i=1}^n -\log(\hat{f}_{Y,\mathbf{z}}(Y_i, \mathbf{z})) \right].$$

Again, leveraging the data-splitting and cross-fitting technique described in Section 7.2 we obtain  $\hat{C}_{X \succ Y | \mathbf{Z} = \mathbf{z}}$  as well as its 95% CI.

To estimate  $\hat{C}_{X \succ Y | \mathbf{Z}}$  we again consider two separate approaches, one for discrete or categorical  $\mathbf{Z}$  and the other for continuous  $\mathbf{Z}$ . First, for discrete or categorical  $\mathbf{Z}$ , (6) implies  $\hat{C}_{X \succ Y | \mathbf{Z}} = \sum_{\mathbf{z} \in \mathcal{Z}} \hat{p}_{\mathbf{Z}}(\mathbf{z}) \hat{C}_{X \succ Y | \mathbf{Z} = \mathbf{z}}$ , where  $\hat{p}_{\mathbf{Z}}$  is the estimated mass function of  $\mathbf{Z}$  and  $\hat{C}_{X \succ Y | \mathbf{Z} = \mathbf{z}}$  is the estimated strata-specific coefficient of asymmetry described above. Under independence of estimated  $\hat{C}_{X \succ Y | \mathbf{Z} = \mathbf{z}}$  across different strata, we obtain a plug-in estimate of  $\hat{C}_{X \succ Y | \mathbf{Z}}$  and further, its 95% CI. For continuous  $\mathbf{Z}$ , noting that  $C_{X \succ Y | \mathbf{Z}} = H(X, \mathbf{Z}) - H(Y, \mathbf{Z})$ , we plug in the estimated densities  $\hat{f}_{X,\mathbf{z}}$  and  $\hat{f}_{Y,\mathbf{z}}$  obtained by **fastMI**

to obtain an estimate of  $\hat{C}_{X \succ Y | \mathbf{Z}}$  as follows:

$$\hat{C}_{X \succ Y | \mathbf{Z}} = \hat{H}(X, \mathbf{Z}) - \hat{H}(Y, \mathbf{Z}) = \frac{1}{n} \sum_{i=1}^n -\log(\hat{f}_{X, \mathbf{Z}}(X_i, \mathbf{Z}_i)) - \frac{1}{n} \sum_{i=1}^n -\log(\hat{f}_{Y, \mathbf{Z}}(Y_i, \mathbf{Z}_i)).$$

Again, leveraging the data-splitting and cross-fitting technique described in Section 7.2 we obtain  $\hat{C}_{X \succ Y | \mathbf{Z}}$  along with a 95% CI.

## 8 Simulation studies

We now report the findings of extensive simulation studies that provide empirical evidence supporting the validity of  $\hat{C}_{X \succ Y}$  to infer strong or weak asymmetry in bivariate  $(X, Y)$ .

### 8.1 Behaviour of $C_{X \succ Y}$ under GEM

In this simulation, we assess the capacity of  $SAC$ , denoted by  $C_{X \succ Y}$ , for measuring the induced asymmetry from a hypothesized  $GEM$  in the strong asymmetry framework when the postulate of Lemma 1 is satisfied. We generate Monte Carlo simulated datasets from  $GEM$  models with or without noise disturbance, each consisting of 1000 *i.i.d.* samples of pairs, where  $GF$   $g$  satisfies Assumption 1 under  $X \sim U(0, 1)$ . We set  $g(x)$  to be one of the following functions:  $x^{1/3}, x^{1/2}, x^2, x^3, \exp(x)$ , and  $\sin(\pi x/2)$ . For each setting, the experiments were repeated  $R = 250$  times to gauge Monte Carlo approximation errors from a set of empirical  $SAC$  values  $\{\tilde{C}_{X \succ Y}^r\}_{r=1}^R$ . We report the mean along with bottom and upper 2.5<sup>th</sup> percentiles of the empirical  $\tilde{C}_{X \succ Y}$  in Table 1. Note that here the empirical

Table 1: Examining mean  $\tilde{C}_{X \succ Y}$  and (2.5%, 97.5%) percentiles in the  $GEM$  framework. We consider uniformly distributed  $X$  and six choices of bijective  $g$ . The first row represents the behaviour of  $C_{X \succ Y}$  in the noise-free  $GEM$  given by  $Y = g(X)$  whereas the subsequent rows examine shifts in the behaviour of  $C_{X \succ Y}$  in the  $NPGE$ M given by  $Y^* = g(X) + \epsilon$ , where  $\mathbb{V}(\epsilon) = \sigma$ .

$\sigma$	$g(x)$					
	$x^{1/3}$	$x^{1/2}$	$x^2$	$x^3$	$\exp(x)$	$\sin(\pi x/2)$
0	0.41 (0.34, 0.48)	0.24 (0.20, 0.28)	0.26 (0.20, 0.33)	0.65 (0.55, 0.77)	0.09 (0.04, 0.14)	0.20 (0.13, 0.27)
0.10	0.21 (0.15, 0.27)	0.09 (0.06, 0.13)	-0.02 (-0.06, 0.02)	0.08 (0.04, 0.12)	-0.04 (-0.08, 0)	-0.16 (-0.3, -0.1)
0.20	-0.04 (-0.1, 0.01)	-0.12 (-0.16, -0.07)	-0.23 (-0.27, -0.2)	-0.18 (-0.23, -0.14)	-0.22 (-0.26, -0.18)	-0.37 (-0.41, -0.33)

value  $\tilde{C}_{X \succ Y}$  approximates the population  $SAC$  under each given  $GEM$ . Further, density estimates of  $\tilde{C}_{X \succ Y}$  in Supplementary Figure 1 show the behaviour of  $SAC$  under each  $NPGE$ M described in Section 4. In all six cases, the average  $\tilde{C}_{X \succ Y}$  reflects the induced

asymmetry under each noise-free *GEM* model. Moreover, both Table 1 and Supplement Figure 1 indicate that the *SAC* can capture the asymmetry in the presence of noise on outcome measurements when the level of noise is low, but gradually loses its capacity when the noise escalates. In addition, the choice of  $g$  influences the *SAC* although  $g$  is not explicitly involved in the calculation of *SAC*; in fact,  $GF$   $g$  only implicitly influences *SAC* via the outcome  $Y$ . These numerical results confirm the theoretical properties and insights in Section 4.

## 8.2 Coverage probability, bias and standard error of $\hat{C}_{X \succ Y}$

In this section 8.2, we use a simulation experiment to show that the proposed estimator  $\hat{C}_{X \succ Y}$  and cross-fitting inference can help detect the induced asymmetry in cases where the identifiability condition given by Assumption 1 may not hold. We simulate data from  $X \sim f_X$  with a present entropy  $H(X)$  and generate  $Y = g(X)$  in a *GEM* via a bijective function  $g$ , with density  $f_Y$  and entropy  $H(Y)$ . We intentionally set  $f_X$  and  $g$  in a way that the induced population-level parameter  $C_{X \succ Y} = H(X) - H(Y)$  is positive while Assumption 1 may fail to hold. We consider two cases that have both closed-form distributions so that the exact true *SAC* is known. (i)  $X \sim \text{Lognormal}(5, 1)$  and  $g(t) := \log(t)$ , which implies  $Y \sim N(5, 1)$  and the true *SAC* = 5; and (ii)  $X \sim \text{Exp}(\mu = 1)$  and  $g(t) := t^{2/3}$ , which implies  $Y \sim \text{Weibull}(\text{scale} = 1, \text{shape} = 3/2)$  and the true *SAC* = 0.213.

Table 2: Examining  $\hat{C}_{X \succ Y}$ : absolute bias (A.Bias), empirical standard error (ESE), the asymptotic SE (ASE) and coverage probability (CP) for different sample sizes  $n \in \{250, 500, 750\}$  under two cases: (i)  $X \sim \text{Lognormal}(5, 1)$  and  $Y \sim N(5, 1)$  and (ii)  $X \sim \text{Exp}(\text{mean} = 1)$  and  $Y \sim \text{Weibull}(\text{scale} = 1, \text{shape} = 3/2)$ .

	Case (I)			Case (II)		
	$n = 250$	$n = 500$	$n = 750$	$n = 250$	$n = 500$	$n = 750$
A.Bias	0.095	0.058	0.048	0.082	0.062	0.049
ESE	0.112	0.073	0.060	0.087	0.064	0.051
ASE	0.114	0.084	0.070	0.102	0.074	0.061
CP	0.945	0.980	0.965	0.935	0.935	0.960

Our simulation is set up as follows: we vary the sample size  $n \in \{250, 500, 750\}$ ; in each case, we obtain both estimate  $\hat{C}_{X \succ Y}$  and asymptotic variance  $\hat{\sigma}_C^2$  according to the formula given in Corollary 1. Then, we construct a 95% asymptotic confidence interval, say  $(\hat{L}_C, \hat{U}_C)$ . Repeating this procedure over  $R = 200$  times, we obtain a set of estimates

$\left\{ \hat{C}_{X \succ Y}(r), \hat{\sigma}_C^2(r) \right\}_{r=1}^R$  as well as the corresponding 95% asymptotic confidence intervals,  $\left\{ (\hat{L}_C(r), \hat{U}_C(r)) \right\}_{r=1}^R$ . Table 2 lists the empirical mean, absolute bias, and standard error of the *SAC* estimates as well as the average of the estimated asymptotic variances. In addition, we report the empirical coverage probability, defined as the proportion of 95% asymptotic confidence intervals covering the true *SAC* parameter. In all the cases considered, our



proposed methodology yields an estimate that has low estimation error. The empirical standard error and average asymptotic standard error are close to each other, confirming the validity of the asymptotic normality given in Corollary 1. More importantly, the coverage probability is close to the nominal 95% level in both scenarios, so the proposed cross-fitting inference is numerically stable and trustful. In summary, these two simulation experiments clearly confirms the large-sample theoretical results given Theorem 3 and Corollary 1.

### 8.3 Comparison of performance of $\hat{C}_{X \succ Y}$ with other causal discovery methods

We compare the accuracy power of our method against three competing methods. The competing methods are the Additive Noise Model (ANM) (Mooij et al., 2016), the Conditional Distribution Similarity (CDS) (Fonollosa, 2019), and the Regression Error-based Causal Inference (RECI) (Blöbaum et al., 2019) approaches. We use the Causal Discovery Toolbox (Kalainathan et al., 2020) to implement these methods, which are used with default parameters supplied by the toolbox.

#### 8.3.1 SIMULATED DATA

We consider uniformly distributed  $X$  and six choices of bijective  $g$ . We generate  $Y = g(X) + \epsilon$ , where  $\mathbb{V}(\epsilon) = \sigma$  and  $\text{Cov}(X, \epsilon) = \rho$ . We draw samples of size  $n = 1000$  repeatedly for  $r = 250$  times and report the proportion of times each method is able to detect the correct directionality  $X \succ Y$  and present our findings in Table 3, which reveals that our method consistently outperform all other methods across all but one simulated data setting.

#### 8.3.2 BENCHMARK DATA

We compared the accuracy of the four competing methods using the `CauseEffectPairs` benchmark that consists of data for  $k = 99$  different cause-effect pairs selected from 37 data sets from various domains (Mooij et al., 2016). Of the 99 pairs, ANM was able to correctly detect 51 pairs and returned inconclusive findings for 18 pairs, while  $\hat{C}_{X \succ Y}$  was able to detect 58 and was inconclusive for 7 pairs. The CDS and RECI approaches proved more successful, correctly detecting 67 and 62 pairs respectively with no inconclusive findings.

## 9 Application

We apply the above asymmetry analytic to study the epigenetic relation between DNA methylation ( $DNAm$ ) and blood pressure ( $BP$ ) that is one of the most important risk factors for cardiovascular disease ( $CVD$ ). We use data from  $n = 522$  children (including 247 boys and 275 girls) aged 10-18 years in the Early Life Exposures in Mexico to Environmental Toxicants (*ELEMENT*) study (Hernandez-Avila et al., 1996). The primary task of scientific interest is to understand potential  $CVD$  causal pathways, part of which involves examining asymmetry between  $DNAm$  alterations and  $CVD$  risks. In this analysis, we examine six candidate genes found to be significantly associated with systolic blood pressure ( $SBP$ ) and diastolic blood pressure ( $DBP$ ) in at least 20 independent studies according to the NHGRI-EBI GWAS Catalog. These six target genes include *FGF5*, *HSD11B2*, *KCNK3*, *ATP2B1*, *ARHGAP42* and *PRDM8*. To investigate their epigenetic roles in  $CVD$ , we investigate

Table 3: Comparing performance of  $\hat{C}_{X \succ Y}$  with competing pairwise causal discovery methods like the Additive Noise Model (ANM), Conditional Distribution Similarity (CDS), and the baseline Regression Error-based Causal Inference (RECI) approaches. We consider uniformly distributed  $X$  and six choices of bijective  $g$ . We generate  $Y = g(X) + \epsilon$ , where  $\mathbb{V}(\epsilon) = \sigma$  and  $\text{Cov}(X, \epsilon) = \rho$ . We draw samples of size  $n = 1000$  repeatedly for  $r = 250$  times and report the proportion of times each method is able to detect the correct directionality  $X \succ Y$ .

$g(x)$	$\sigma$	$\rho$	Accuracy			
			$\hat{C}_{X \succ Y}$	ANM	CDS	REI
$x^{1/3}$	0	0	<b>1.00</b>	0.22	0.00	0.00
	0.05	0.10	<b>1.00</b>	0.24	0.00	0.00
	0.05	0.60	<b>1.00</b>	0.21	0.00	0.00
$x^{1/2}$	0	0	<b>1.00</b>	0.18	0.00	0.00
	0.05	0.10	<b>1.00</b>	0.22	0.00	0.00
	0.05	0.60	<b>1.00</b>	0.18	0.00	0.00
$x^2$	0	0	<b>1.00</b>	0.24	<b>1.00</b>	<b>1.00</b>
	0.05	0.10	<b>1.00</b>	0.18	<b>1.00</b>	<b>1.00</b>
	0.05	0.60	<b>1.00</b>	0.20	<b>1.00</b>	<b>1.00</b>
$x^3$	0	0	<b>1.00</b>	0.20	0.00	<b>1.00</b>
	0.05	0.10	<b>1.00</b>	0.20	0.02	<b>1.00</b>
	0.05	0.60	<b>1.00</b>	0.18	0.00	<b>1.00</b>
$\exp(x)$	0	0	<b>1.00</b>	0.22	0.00	<b>1.00</b>
	0.05	0.10	<b>1.00</b>	0.20	0.44	<b>1.00</b>
	0.05	0.60	0.98	0.21	0.05	<b>1.00</b>
$\sin(\pi x/2)$	0	0	<b>1.00</b>	0.24	<b>1.00</b>	0.00
	0.05	0.10	<b>1.00</b>	0.26	<b>1.00</b>	0.00
	0.05	0.60	<b>1.00</b>	0.26	<b>1.00</b>	0.00

whether  $\beta$  values of *DNAm* (specifically, cytosine-phosphate-guanine (CpG) methylation) influence change in *BP* or if the converse is true (Dicorpo et al., 2018; Hong et al., 2023).

To perform a gene-level analysis, we average  $\beta$  values of *DNAm* over CpG sites within each gene, which is then normalized across subjects by an affine transformation described in Section 2.1 to minimize any undue influence of location or scale changes in individual *DNAm* measurements. The same normalization procedure is applied to *SBP* and *DBP* measurements. We apply the *GEM* approach to conduct the asymmetry analysis with or without sex-stratification.

First, we consider a hypothesized *GEM*:  $\text{DNAm} = g(\text{BP}, \text{sex})$ , where *DNAm* denotes normalized average beta value of one gene and *BP* may be normalized *SBP* or *DBP*, and sex-stratification may or may not be used in the analysis. When sex is included as a confounder

in the analysis, its mass function is estimated by  $\hat{p}_{\text{sex}}(\text{boy}) = 247/(247 + 275) = 0.47$  and  $\hat{p}_{\text{sex}}(\text{girl}) = 0.53$ . Under this null model of asymmetry, in the case without sex-stratification (the sample size  $n = 522$ ), our cross-fitting inference method has identified the *GEM*-induced asymmetry from three genes, namely *FGF5*, *HSD11B2*, and *PRDM8*, at the significance level 0.05. Among these identified genes, we further conduct a sex-stratified analysis that yields the same findings; see Supplementary Figure 3 that reports the cross-inference results for all six genes in our candidate study. Moreover, if the null *GEM* is rejected we further examine if the opposite directionality exists under an inverse *GEM*:  $BP = g(\text{DNAm}, \text{sex})$ ; see Supplementary Figure 4 for the cross-inference results.

Here is a summary of our major findings. Cross-fitting inference results in Supplementary Figure 3 support the directionality from both diastolic and systolic *BP* to *DNAm* of two genes, *FGF5* and *HSD11B2* for both males and females. In contrast, Supplementary Figure 4 indicates the opposite directionality from *DNAm* of gene *PRDM8* to diastolic *BP* in the unstratified analysis and for girls. However, there is no evidence for directionality between systolic *BP* and *DNAm* in *PRDM8*. Further, we checked if the tolerance of noise contamination on the *BP* measurements is controlled by the bound of Remark 5. See the appendix for more details on the noise tolerance analysis. Our investigations reveal that the noise perturbation has little influence on the results drawn from our inference method.

Our inference method unveils novel pathways from *BP* to *DNAm* for two genes *FGF5* and *HSD11B2*. *FGF5* is reported in Domouzoglou et al. (2015) as a key gene in several animal studies that increases myocardial blood flow and function, decrease myocyte apoptosis, and increase myocyte number after gene transfer of the growth factor. However, there are no available results of its effects in human cardiovascular disease. Our analysis is the first to unveil a pathway from changes in *BP* to regulate *DNAm* of this key CVD gene in a human cohort study. Gene *HSD11B2* was reported in Rahman et al. (2011) to be associated with obesity-related cardiovascular risk factors, e.g. type II diabetes and hypertension. Hypertension is often associated with chronic inflammation and oxidative stress, both of which can trigger an imbalance in the immune system. This can, in turn, modulate a person’s methylation patterns. In summary, these new findings confer an added sense of directionality in the study of *BP* variation and epigenetic biomarkers, paving the way for future advancements in individualized risk assessments and even therapeutic targets.

## 10 Concluding remarks

Asymmetry is an inherent property of bivariate associations and therefore must not be ignored (Zheng et al., 2012). In this paper, we present a new methodology in the framework of generative exposure mapping (*GEM*) models so that the induced asymmetry between two random variables  $X$  and  $Y$  is captured by an information-theoretic coefficient  $C_{X \succ Y}$ . Utilizing this asymmetry measure, we develop a cross-fitting inference that enables us to examine a certain hypothesized directionality with proper uncertainty quantification. The intrinsic linkage between information theory and an experiment with a uniformly distributed exposure provides an interesting insight into asymmetry from the perspective of causality, where we argue that the induced asymmetry from a *GEM* model may be regarded as a low-dimensional imprint of causality. Further, simulation studies reveal that if  $X$  is uniformly generated, the asymmetry measure  $C_{X \succ Y}$  can detect different dynamics of outcomes under

different GEMs without actually estimating the mapping functions, and such capacity prevails in noise-perturbed *GEM* models. It is worth noting that such an extension requires one assumption of the contamination error being independent of the exposure. A potential area of future work would involve addressing endogeneity in contaminated *GEM* models with correlations between the errors and exposure (Breunig and Burauel, 2021), in which the instrumental variable technique is worth exploring.

A main contribution of this paper pertains to filling in a technical gap by providing uncertainty quantification in the study of directionality (Daniušis et al., 2010) through cross-fitting inference methods. Theoretical guarantees are rigorously established with key large-sample properties through asymptotic behavior for estimated functionals of probability density functions, which have been implemented by a fast-Fourier transformation technique to avoid the parameter tuning (i.e. bandwidth selection) to improve computational speed. Our proposed approach has the flexibility to incorporate confounding factors  $\mathbf{Z}$  into asymmetry measures, which is useful for performing meaningful subgroup analyses. Albeit the current limitation of low-dimensional confounding allowed, the framework is extendable to embrace high-dimensional confounders via, for example, deep learning (*DL*) based generative machinery proposed by Zhou et al. (2023). The *DL* method generates random samples from target conditional distributions and may be seamlessly integrated into our inference method in which we utilize random samples from the target conditional distribution of  $(X, Y) | \mathbf{Z}$  for high dimensional  $\mathbf{Z}$  in the calculation of test statistics.

Several further applications and extensions of the proposed  $C_{X \succ Y}$  measure and cross-fitting inference method are worth exploring, including the extension of *GEM*-induced asymmetry in functional or longitudinal variables; for example, the found asymmetries between *DNA*m and *BP* in our data analysis would become more reliable if repeated measurements of *BP* are available. Our framework may be used either as a discovery or confirmatory tool in the pathway study under certain directed graphs, thereby aiding practitioners in improving the rigor and reproducibility of scientific research.

## Acknowledgments and Disclosure of Funding

This work is partially supported by NSF DMS-2113564 and NIH R01ES033656 (for Song), and the University of Michigan Rackham Predoctoral Fellowship (for Purkayastha). All code and data related to this manuscript are available online on [Github](#).

## Appendix I: Proofs

### I. Proof of Theorem 1

**Proof** Note that de Bruijn's identity (Barron, 1986, Proof of Lemma 1) states that  $\frac{\delta H(Y + \sqrt{t}Z)}{\delta t} = \frac{I(Y + \sqrt{t}Z)}{2}$ . In other words,  $H(Y + \sqrt{t}Z)$  is an increasing function of  $t$  as  $I(Y + \sqrt{t}Z) > 0$  for all  $t > 0$ . Hence, there exists  $\sigma'$ , such that  $H(Y + \epsilon) \leq H(Y + \sqrt{\sigma'}Z)$ . Further, from the fundamental theorem of calculus, note that

$$H(Y + \sqrt{\sigma'}Z) - H(Y) = \frac{1}{2} \int_0^{\sigma'} I(Y + \sqrt{t'}Z) dt'.$$

We use convolution inequality of Fisher information (Zamir, 1998, Theorem 1) given by:

$$I(Y + \sqrt{t}Z) \leq \frac{I(Y)I(\sqrt{t}Z)}{I(Y) + I(\sqrt{t}Z)},$$

and note that  $I(\sqrt{t}Z) = 1/t$  to obtain the following inequality:

$$H(Y + \sqrt{\sigma'}Z) \leq H(Y) + \frac{1}{2} \log(\sigma' I(Y) + 1).$$

■

### II. Proof of Theorem 3

**Proof** From Theorem 2, for any small  $\epsilon$ , there exists sufficiently large  $n$  such that

$$\left| \hat{f}_{X;1}(x) - f_X(x) \right| < \epsilon, \text{ and } \left| \hat{f}_{X;2}(x) - f_X(x) \right| < \epsilon, \quad x \in \mathbb{R}.$$

Next, note that if  $|x - a| < a$  for  $a > 0$ , i.e., if  $|x/a - 1| < 1$ , the following Taylor series expansion holds:

$$\ln(x) - \ln(a) = \sum_{n=1}^{\infty} \frac{(-1)^{n-1}}{na^n} (x - a)^n = \frac{1}{a}(x - a) - \frac{1}{2a^2}(x - a)^2 + \frac{1}{3a^3}(x - a)^3 + \dots$$

Since, from Theorem 2,  $\hat{f}_X$  is uniformly consistent for  $f_X$ , we neglect quadratic and higher terms in the above expression and write the following approximations for  $j \in 1, \dots, n$ :

$$\begin{aligned} \ln \left( \hat{f}_{X;1}(X_{n+j}) \right) &= \ln \left( f_{X;1}(X_{n+j}) \right) + \frac{\hat{f}_{X;1}(X_{n+j}) - f_{X;1}(X_{n+j})}{f_{X;1}(X_{n+j})}, \\ \ln \left( \hat{f}_{X;2}(X_j) \right) &= \ln \left( f_{X;2}(X_j) \right) + \frac{\hat{f}_{X;2}(X_j) - f_{X;2}(X_j)}{f_{X;2}(X_j)}. \end{aligned}$$

By Assumption 5,  $f_X$  is bounded below by a constant, say  $B^{-1}$ , on its support, it is easy to show that

$$\begin{aligned} \left| \hat{H}_1(X) - H_{0;1}(X) \right| &\leq \frac{1}{n} \sum_{j=1}^n \left| \frac{\hat{f}_{X;2}(X_j) - f_X(X_j)}{f_X(X_j)} \right| \leq \frac{\epsilon}{B}, \\ \left| \hat{H}_2(X) - H_{0;2}(X) \right| &\leq \frac{1}{n} \sum_{j=1}^n \left| \frac{\hat{f}_{X;1}(X_{n+j}) - f_X(X_{n+j})}{f_X(X_{n+j})} \right| \leq \frac{\epsilon}{B}, \end{aligned}$$

which together imply  $\left| \hat{H}(X) - H_0(X) \right| \xrightarrow{a.s.} 0$ , as  $n \rightarrow \infty$ . Further, the strong law of large numbers implies as  $n \rightarrow \infty$ , we have  $H_0(X) - H(X) \xrightarrow{a.s.} 0$ . Hence, using the inequality obtained above in conjunction with the strong law of large numbers yields  $\hat{H}(X) - H(X) \xrightarrow{a.s.} 0$  as  $n \rightarrow \infty$ . Similar results hold for  $\hat{H}_Y$ ; thus, invoking the continuous mapping theorem, we are able to show  $\hat{C}_{X>Y} \xrightarrow{a.s.} C_{X>Y}$  as  $n \rightarrow \infty$ . This concludes the proof.  $\blacksquare$

### III. Proof of Theorem 4

**Proof** We consider the following Taylor series expansion:

$$\begin{aligned} \sqrt{n} \left\{ \hat{H}_2(X) - H_{0;2}(X) \right\} &= \frac{1}{\sqrt{n}} \sum_{j=1}^n \left\{ \frac{\hat{f}_{X;1}(X_{n+j}) - f_{X;1}(X_{n+j})}{f_{X;1}(X_{n+j})} \right\} + o_P(n^{-1/2}) \\ &= \frac{S_n(2)}{\sqrt{n}} + o_P(n^{-1/2}). \end{aligned}$$

We now show that the leading term  $S_n(2)/\sqrt{n} \xrightarrow{P} 0$  as  $n \rightarrow \infty$ , which will establish

$$\sqrt{n} \left\{ \hat{H}_2(X) - H_{0;2}(X) \right\} \xrightarrow{P} 0, \quad \text{as } n \rightarrow \infty.$$

Using identical arguments, we establish similar results for  $\hat{H}_2(Y)$  as well. It is sufficient to show  $\mathbb{E} \left[ \left\{ S_n(2)/\sqrt{n} \right\}^2 \right] \rightarrow 0$  as  $n \rightarrow \infty$ . Note that  $\mathbb{E} \left[ \left\{ S_n(2)/\sqrt{n} \right\}^2 \right] = \mathbb{E}^2 \left[ \left\{ S_n(2)/\sqrt{n} \right\} \right] + \mathbb{V} \left[ \left\{ S_n(2)/\sqrt{n} \right\} \right]$ . First, we prove  $\mathbb{E} \left[ \left\{ S_n(2)/\sqrt{n} \right\} \right]$ :

$$\begin{aligned} \mathbb{E} \left\{ \frac{S_n(2)}{\sqrt{n}} \right\} &= \mathbb{E}_{\mathcal{D}_1} \left[ \mathbb{E}_{\mathcal{D}_2 | \mathcal{D}_1} \left\{ \frac{S_n(2)}{\sqrt{n}} \middle| \mathcal{D}_1 \right\} \right] \\ &= \mathbb{E}_{\mathcal{D}_1} \left[ \mathbb{E}_{\mathcal{D}_2 | \mathcal{D}_1} \left\{ \frac{1}{\sqrt{n}} \sum_{j=1}^n \left( \frac{\hat{f}_{X;1}(X_{n+j}) - f_X(X_{n+j})}{f_X(X_{n+j})} \right) \middle| \mathcal{D}_1 \right\} \right] \\ &= \sqrt{n} \mathbb{E}_{\mathcal{D}_1} \left[ \mathbb{E}_{\mathcal{D}_2 | \mathcal{D}_1} \left\{ \left( \frac{\hat{f}_{X;1}(X) - f_X(X)}{f_X(X)} \right) \middle| \mathcal{D}_1 \right\} \right], \end{aligned}$$

where the inner expectation term is evaluated as follows:

$$\mathbb{E}_{\mathcal{D}_2 | \mathcal{D}_1} \left\{ \left( \frac{\hat{f}_{X;1}(X) - f_X(X)}{f_X(X)} \right) \middle| \mathcal{D}_1 \right\} = \int_{\mathbb{R}} \left( \frac{\hat{f}_{X;1}(x) - f_X(x)}{f_X(x)} \right) f_X(x) dx = 0,$$

where the equality holds since  $\hat{\phi}_1$  is the Fourier transform associated with the optimal density function estimator  $\hat{f}_{X;1}$ , and we know  $\int_{\mathbb{R}} \hat{f}_{X;1}(x) dx = \hat{\phi}_1(0) = 1$  and consequently,  $\mathbb{E}[\{S_n(2)/\sqrt{n}\}] = 0$ . Next, we consider the term  $\mathbb{V}[\{S_n(2)/\sqrt{n}\}]$ :

$$\mathbb{V} \left[ \left\{ \frac{S_n(2)}{\sqrt{n}} \right\} \right] = \mathbb{E}_{\mathcal{D}_1} \left[ \mathbb{V}_{\mathcal{D}_2|\mathcal{D}_1} \left\{ \left( \frac{S_n(2)}{\sqrt{n}} \right) \middle| \mathcal{D}_1 \right\} \right] + \mathbb{V}_{\mathcal{D}_1} \left[ \mathbb{E}_{\mathcal{D}_2|\mathcal{D}_1} \left\{ \left( \frac{S_n(2)}{\sqrt{n}} \right) \middle| \mathcal{D}_1 \right\} \right],$$

where the second term is zero, as per our calculations above. Conditional on  $\mathcal{D}_1$ , the terms  $\hat{f}_{X;1}(X_{n+j})$  are independent and identically distributed for  $1 \leq j \leq n$ . We have:

$$\begin{aligned} \mathbb{V}_{\mathcal{D}_2|\mathcal{D}_1} \left\{ \left( \frac{S_n(2)}{\sqrt{n}} \right) \middle| \mathcal{D}_1 \right\} &= \mathbb{V}_{\mathcal{D}_2|\mathcal{D}_1} \left\{ \frac{1}{\sqrt{n}} \sum_{j=1}^n \left( \frac{\hat{f}_{X;1}(X_{n+j}) - f_X(X_{n+j})}{f_X(X_{n+j})} \right) \middle| \mathcal{D}_1 \right\} \\ &= \mathbb{V}_{\mathcal{D}_2|\mathcal{D}_1} \left\{ \left( \frac{\hat{f}_{X;1}(X) - f_X(X)}{f_X(X)} \right) \middle| \mathcal{D}_1 \right\} \\ &= \mathbb{E}_{\mathcal{D}_2|\mathcal{D}_1} \left\{ \left( \frac{\hat{f}_{X;1}(X) - f_X(X)}{f_X(X)} \right)^2 \middle| \mathcal{D}_1 \right\}, \end{aligned}$$

The last equality follows from

$$\mathbb{E}_{\mathcal{D}_2|\mathcal{D}_1} \left\{ \left( \frac{\hat{f}_{X;1}(X) - f_X(X)}{f_X(X)} \right) \middle| \mathcal{D}_1 \right\} = 0.$$

Moreover,

$$\mathbb{E}_{\mathcal{D}_2|\mathcal{D}_1} \left\{ \left( \frac{\hat{f}_{X;1}(X) - f_X(X)}{f_X(X)} \right)^2 \middle| \mathcal{D}_1 \right\} \leq B \int_{\mathbb{R}} (\hat{f}_{X;1}(x) - f_X(x))^2 dx.$$

where  $B$  is a (positive) lower bound for the density  $f_X$  over its support. Consequently, we get

$$\mathbb{V}[\{S_n(2)/\sqrt{n}\}] \leq B \times \mathbb{E}_{\mathcal{D}_1} \left\{ \int_{\mathbb{R}} (\hat{f}_{X;1}(x) - f_X(x))^2 dx \right\} = B \times MISE(\hat{f}_{X;1}, f_X).$$

Bernacchia and Pigolotti (2011) present an expression of *MISE* in terms of the optimal kernel and prove that the last expression goes to zero as sample size increases, i.e.,  $MISE(\hat{f}_{X;1}, f_X) \rightarrow 0$  as  $n \rightarrow \infty$ . This allows us to claim  $\sqrt{n} \left( \hat{H}_2(X) - H_{0;2}(X) \right) \xrightarrow{\mathcal{P}} 0$  as  $n \rightarrow \infty$ . Note that the arguments presented above are generally valid for any true density function that is bounded away from zero and infinity on its support. Hence, they can also be used to establish similar results involving  $\sqrt{n} \left( \hat{H}_2(Y) - H_{0;2}(Y) \right) \xrightarrow{\mathcal{P}} 0$  as  $n \rightarrow \infty$ .

Note that we can interchange the roles of  $\mathcal{D}_1$  and  $\mathcal{D}_2$  in the proof above to arrive at

$$\sqrt{n} \begin{pmatrix} \hat{H}_1(X) - H_{0;1}(X) \\ \hat{H}_1(Y) - H_{0;1}(Y) \end{pmatrix} \xrightarrow{\mathcal{P}} 0, \text{ as } n \rightarrow \infty, \quad (13)$$

which can be combined with the result we have obtained, given by:

$$\sqrt{n} \begin{pmatrix} \hat{H}_2(X) - H_{0;2}(X) \\ \hat{H}_2(Y) - H_{0;2}(Y) \end{pmatrix} \xrightarrow{\mathcal{P}} 0, \text{ as } n \rightarrow \infty,$$

and the continuous mapping theorem to yield the following:

$$\sqrt{n} \begin{pmatrix} \hat{H}(X) - H_0(X) \\ \hat{H}(Y) - H_0(Y) \end{pmatrix} \xrightarrow{\mathcal{P}} 0, \text{ as } n \rightarrow \infty.$$

This concludes the proof. ■

#### IV. Proof of Corrolary 1

**Proof** Using Theorem 4 and Lemma 2 in conjunction with Slutsky's theorem, we get

$$\sqrt{n} \begin{pmatrix} \hat{H}(X) - H(X) \\ \hat{H}(Y) - H(Y) \end{pmatrix} \xrightarrow{\mathcal{D}} N(\mathbf{0}, \Sigma), \text{ as } n \rightarrow \infty,$$

where  $\Sigma$  is the  $2 \times 2$  dispersion matrix of  $(H_0(X), H_0(Y))'$ . Hence, we note that

$$\sqrt{n} \left( \hat{C}_{X \succ Y} - C_{X \succ Y} \right) \xrightarrow{\mathcal{D}} N(0, \sigma_C^2), \text{ as } n \rightarrow \infty.$$

This concludes the proof. ■

#### Appendix II: Behaviour of $\hat{C}_{X \succ Y}$ in *NPGEMs*

#### Appendix III: Behaviour of $\hat{C}_{X \succ Y}$ under weak asymmetry

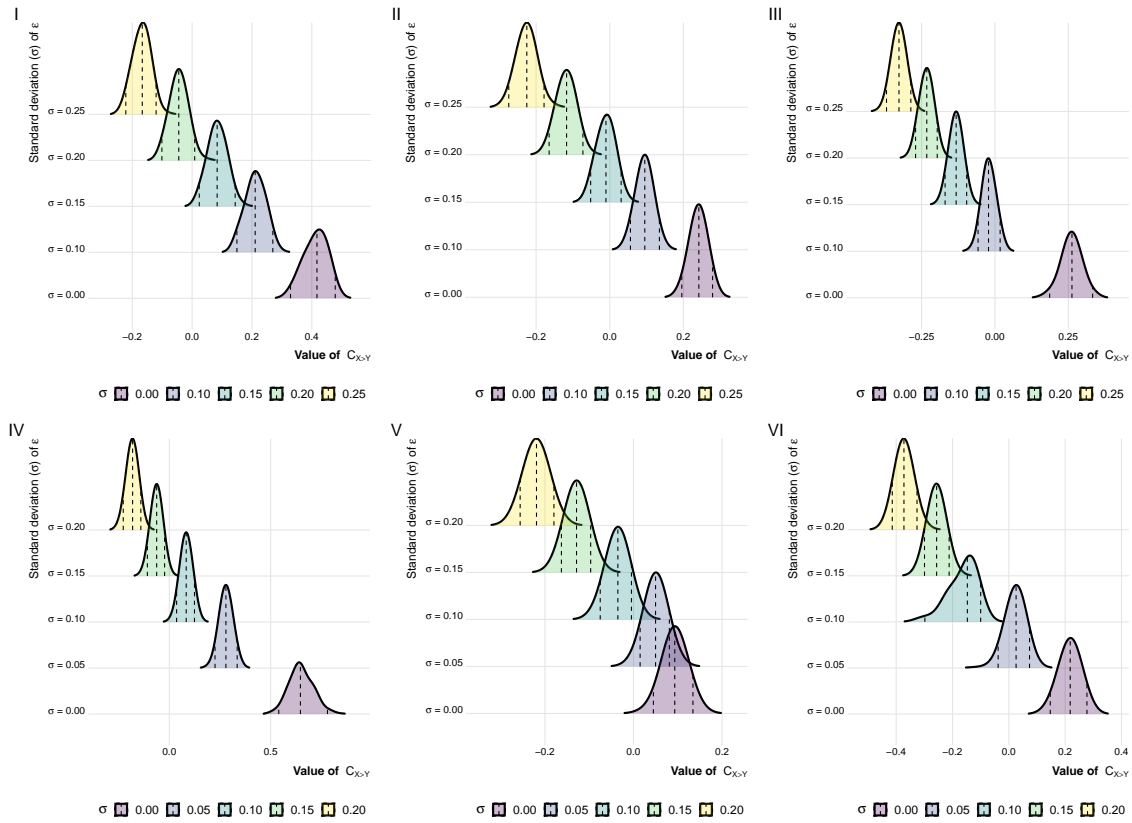
##### Simulation 3

Using the *WAC*,  $C_{X \succ Y}$ , we want to evaluate its sensitivity for the departure from symmetric associations in synthetic bivariate data within our framework of weak asymmetry in the absence of a *GEM*. We generate a sample of  $n = 500$  observations drawn from a bivariate copula dependence model with PDF  $f_{XY}$  on  $\mathbb{R}^2$  according to Sklar's theorem. We specify the underlying copula dependence model and the two associated marginal densities, given as follows:

1. **Choice of copula dependence model:** we choose the bivariate Gaussian copula with correlation parameter  $\rho = 0.25$  (Song, 2007).
2. **Choice of marginals:** choice of the marginal densities influences predictive asymmetry in the proposed information-theoretic framework. We consider the Gaussian  $N(0, \sigma^2)$ ,  $\text{Exp}(\mu = 1/\lambda)$ , and  $\text{Lognormal}(\text{scale} = \gamma)$  density functions. We vary the parameters  $\sigma$ ,  $\lambda$  and  $\gamma$  over a range of values.



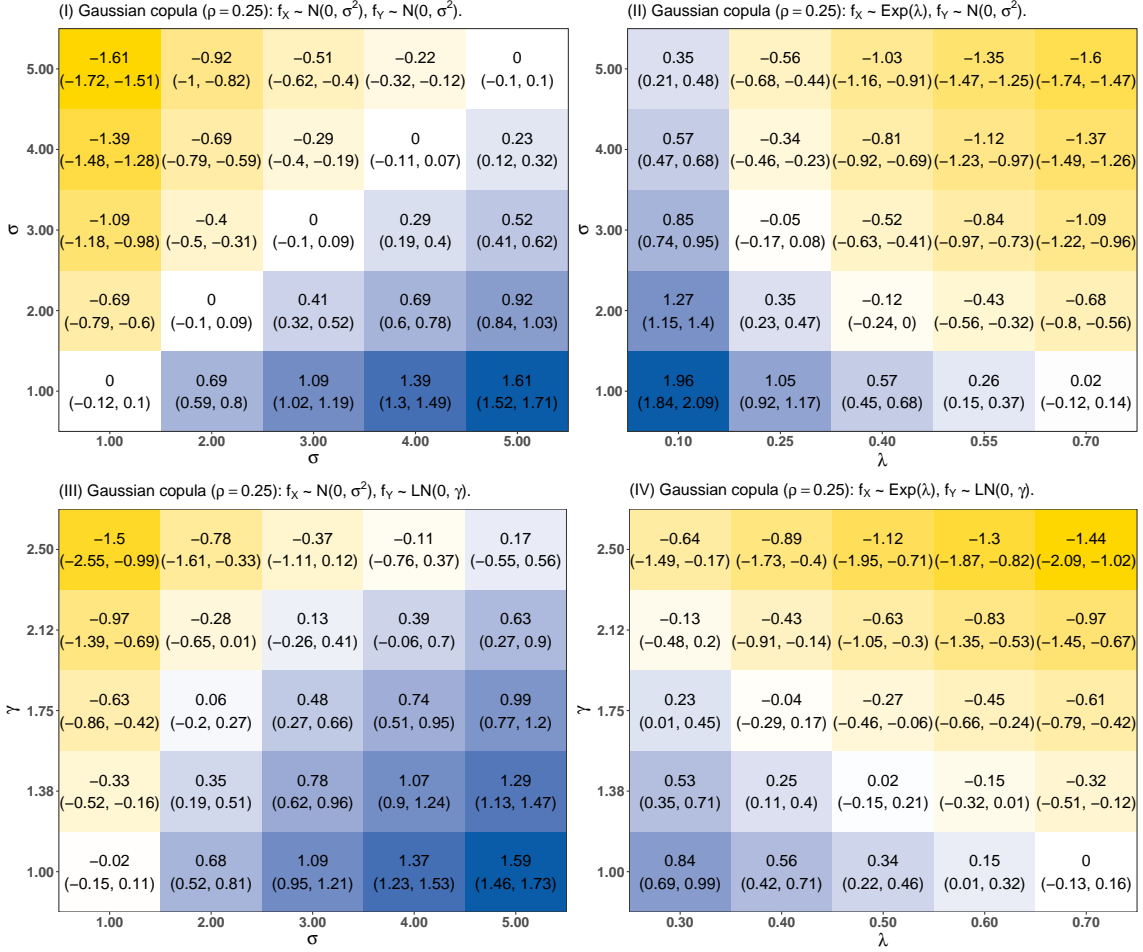
Behaviour of  $C_{X \succ Y}$  in the GEM model  $Y = f(X) + \varepsilon$ , where  $X \sim U(0, 1)$  and  $\varepsilon \sim N(0, \sigma^2)$ . Smoothed density estimates of  $C_{X \succ Y}$  are stratified by standard deviation ( $\sigma$ ) of contaminating noise  $\varepsilon$ .  
 Case I:  $f(x) = x^{1/2}$ , II:  $f(x) = x^{1/3}$ , III:  $f(x) = x^2$ , IV:  $f(x) = x^3$ , V:  $f(x) = \exp(x)$ , VI:  $f(x) = \sin(x)$ . Dashed vertical lines in each density plot correspond to 2.5th, 50th and 97.5th percentiles of each distribution.



Supplementary Figure 1: Examining the behaviour of  $\hat{C}_{X \succ Y}$  under possibly contaminated *GEMs*.

**Joint distribution is specified by Gaussian copula with parameter  $\rho = 0.25$ .**

For each marginal parameter combination, we report  $\hat{C}$  (95% CI).



Supplementary Figure 2: Examining the behaviour of  $\hat{C}_{X \succ Y}$  under weak asymmetry framework.

Note that increasing the scale parameter  $\gamma$  for the lognormal distribution and the dispersion parameter  $\sigma$  for the Gaussian distribution yields increased entropy values. In contrast, increasing the rate parameter  $\lambda$  for the exponential distribution yields decreased entropy values. For a given association value we generate bivariate *i.i.d.* samples on  $(X, Y)$ , each of size  $n = 500$ . For each simulated sample, we aggregate the estimated  $WAC$ s  $\{\hat{C}_{X \succ Y}^r\}_{r=1}^R$  for a total of  $R = 200$  iterations. We report the aggregated mean from the set of estimates in addition to the 2.5-th and 97.5-th percentiles as the lower and upper quantile-based 95% confidence intervals of  $\hat{C}_{X \succ Y}$ .

Subplots (I), (II), (III), and (IV) of Figure 2 examine behaviour of  $\hat{C}_{X \succ Y}$  upon changing the marginal parameters. In this way we evaluate how the  $WAC$   $\hat{C}_{X \succ Y}$  captures departure from balanced marginal entropy values in our weak asymmetry framework in these bivariate

models. Our simulation results vary based on how we specify the marginal density functions, which in turn influences the underlying marginal entropy.

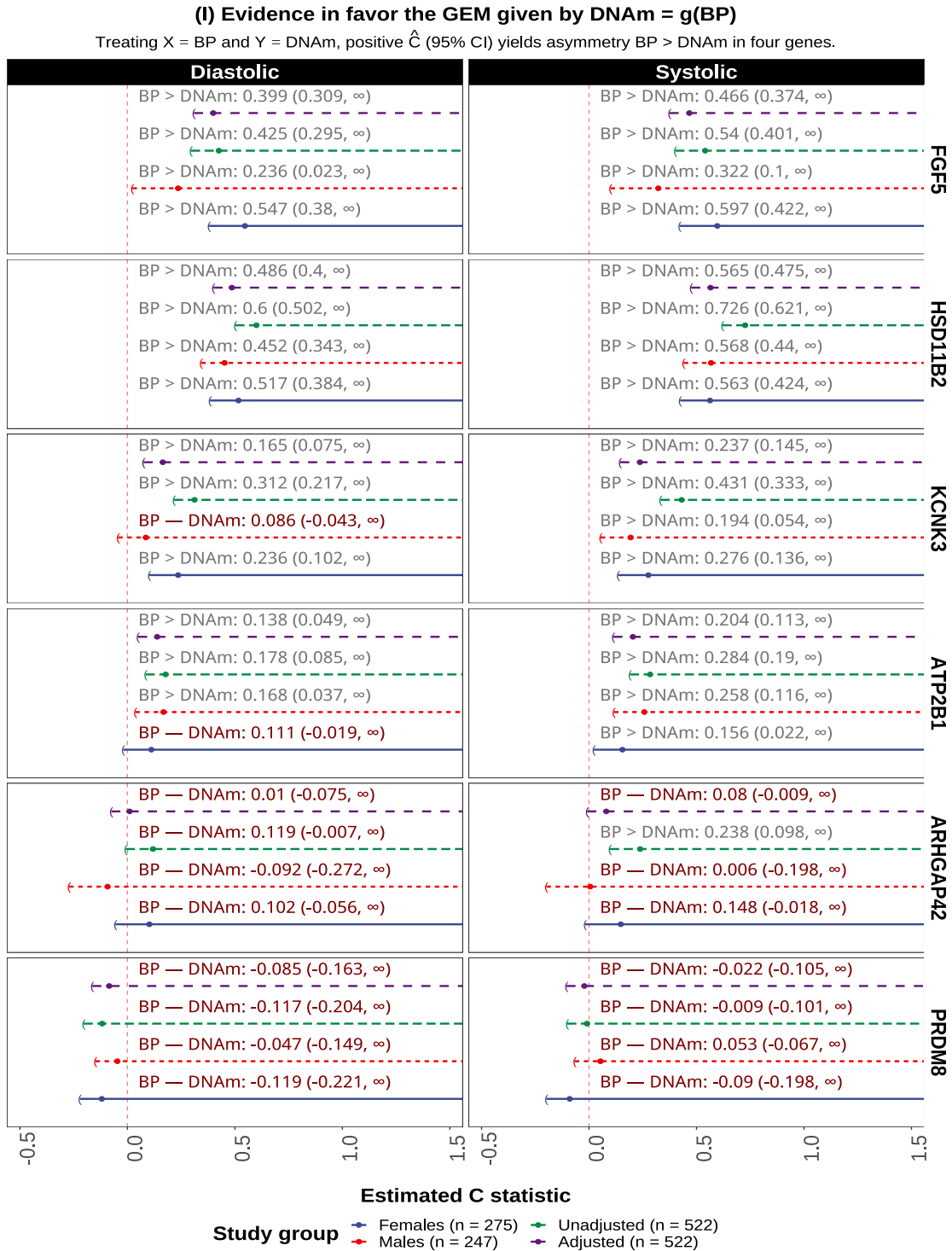
In cases (I) and (III), note that increasing the  $X$ -marginal parameter while keeping the  $Y$ -marginal fixed causes the entropy of  $X$  to rise, relative to  $Y$ , thereby causing an increase in the value of  $\hat{C}_{X \succ Y}$ . In contrast, in cases (II) and (IV), note that increasing the  $X$ -marginal parameter while keeping the  $Y$ -marginal fixed causes the entropy of  $X$  to fall, relative to  $Y$ , thereby causing a decrease in the value of  $\hat{C}_{X \succ Y}$ .

## Appendix IV: Additional material for application to methylation data

See Figures 3 and 4 for cross-inference results on all six genes. We summarise our major findings here:

1. Weak/no signal for  $BP \rightarrow DNAm$  in  $PRDM8$  and  $ARHGAP42$  in Figure 3. When checking for evidence to support the opposite direction  $DNAm \rightarrow BP$  for the same genes, we only find significant  $\hat{C}_{DNAm \succ DBP}$  for males in  $PRDM8$ .
2. Simpson’s paradox for  $DBP \rightarrow DNAm$  in  $ARHGAP42$ : Note in Figure 3 how conditioning on sex removes significant directionality whereas the sex-unadjusted coefficient reveals directionality.
3. Figure 3 support the directionality from both diastolic and systolic BP to DNAm of two genes,  $FGF5$  and  $HSD11B2$ . In contrast, Figure 4 indicates the opposite directionality from DNAm of gene  $PRDM8$  to diastolic BP in the unstratified analysis and the group of girls. However, there is no evidence for directionality between systolic BP and DNAm in  $PRDM8$ .

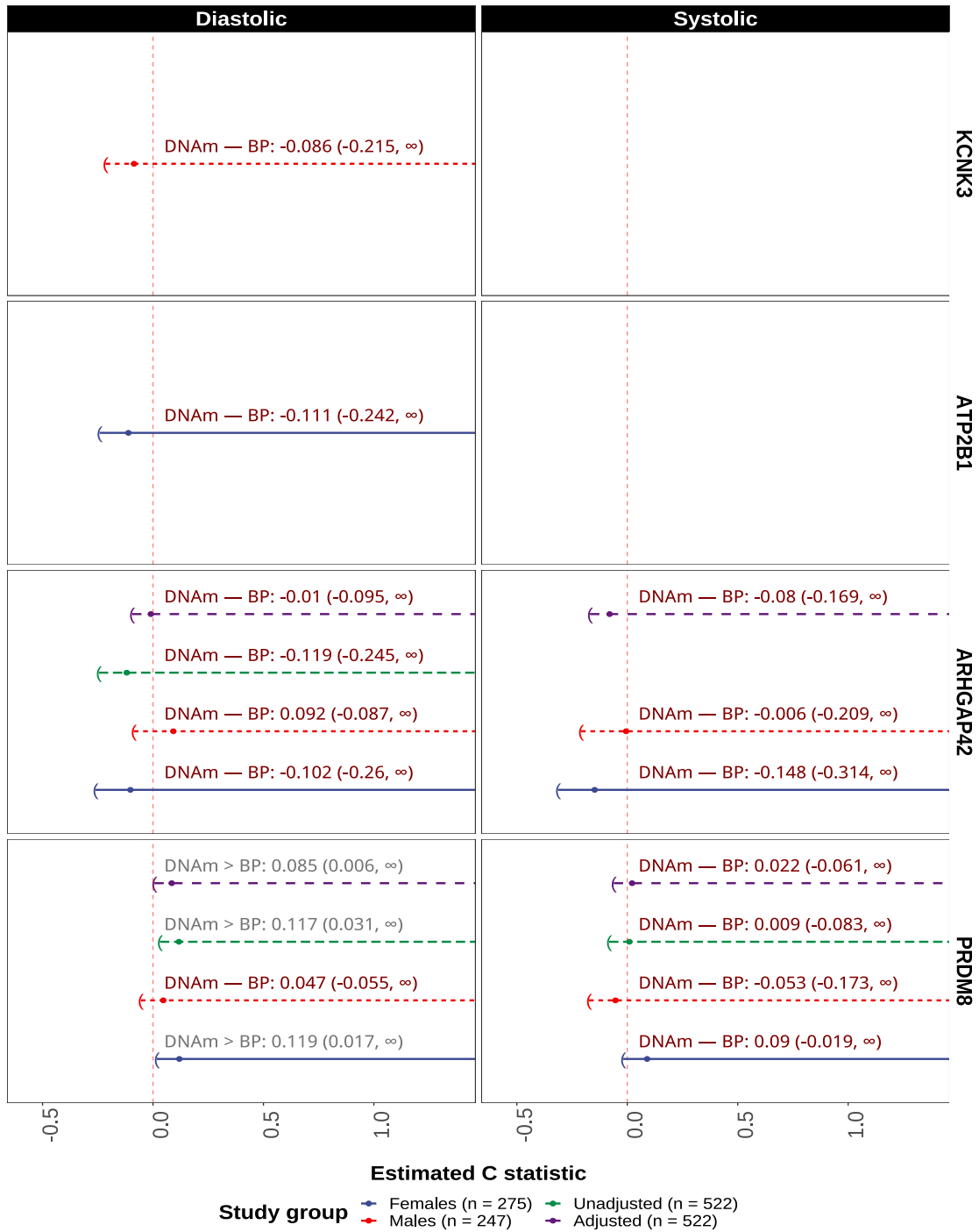
To empirically check if the tolerance of normally distributed noise contamination on the  $BP$  measurements is controlled by the bound of Remark 5, we fitted a linear generalised additive model ( $GAM$ ) with linear splines to estimate  $\hat{g}$  so that the resulting  $\hat{g}$  is a bijective function. Using the fitted mode and residuals, we can estimate  $\hat{I}(\hat{Y})$  and  $\hat{C}_{X \succ Y} = \hat{H}(X) - \hat{H}(\hat{Y})$ , and then obtained the estimated critical value  $\hat{\sigma}_{CRIT} = (\exp(2\hat{C}_{X \succ Y}) - 1) / \hat{I}(\hat{Y})$  as well as the residual variance  $\hat{\sigma}$ . We present a tabular summary of the bootstrapped distribution of  $\hat{\sigma} - \hat{\sigma}_{CRIT}$  in Table 4. According to Section 4 of the main article, our method correctly captures the direction induced by the  $NPGEM$  so long as  $\hat{\sigma}$  and  $\hat{\sigma}_{CRIT}$  are comparable. We implement a bootstrap approach to test whether  $\sigma$  and  $\sigma_{CRIT}$  and present our findings in Table 4. This approach is *not* a rigorous test, but rather a diagnostic tool to examine noise contamination relative to signal in the data. From Table 4 we see that in most cases the estimated  $\hat{\sigma}$  and  $\hat{\sigma}_{CRIT}$  are comparable since most of bootstrap-based 95% CIs of  $\hat{\sigma}_{CRIT} - \hat{\sigma}$  contains zero. There are only a few cases where there is some evidence to reverse the inequality of  $\sigma \leq \sigma_{CRIT}$ , namely in  $ARHGAP42$  for males,  $KCNK3$  for males, and finally in  $PRDM8$  for males. Although the significant 95% CIs are very close to zero, our findings imply that we exercise caution with examining asymmetry in an  $NPGEM$  framework using the strong asymmetry coefficient.



Supplementary Figure 3: Cross-fitting inference results for asymmetry in  $BP$  and  $DNAm$  include unadjusted  $\hat{C}_{BP > DNAm}$  along with sex-adjusted  $\hat{C}_{BP > DNAm|sex}$  for six candidate genes.

**(II) Evidence in favor the GEM given by BP = h(DNA<sub>m</sub>)**

Treating X = DNA<sub>m</sub> and Y = BP, positive  $\hat{C}$  (95% CI) yields asymmetry DNA<sub>m</sub> > BP in PRDM8.



Supplementary Figure 4: Cross-fitting inference results for asymmetry in *BP* and *DNA<sub>m</sub>* include unadjusted  $\hat{C}_{DNA_m > BP}$  along with sex-adjusted  $\hat{C}_{DNA_m > BP|sex}$  for six candidate genes.

Gene	BP	Group	95% bootstrap CI for $\hat{\sigma}_{CRIT} - \hat{\sigma}$
<i>FGF5</i>	Systolic	Females	(-0.138, 0.268)
		Males	(-0.170, 0.001)
		Combined	(-0.145, 0.071)
	Diastolic	Females	(-0.140, 0.549)
		Males	(-0.177, 0.060)
		Combined	(-0.162, 0.173)
<i>HSD11B2</i>	Systolic	Females	(-0.105, 0.528)
		Males	(-2.611, 1.671)
		Combined	(-3.400, 3.498)
	Diastolic	Females	(-0.101, 0.691)
		Males	(-0.162, 0.277)
		Combined	(-3.400, 3.498)
<i>ARHGAP42</i>	Systolic	Females	(-0.827, 0.262)
		Males	(-0.191, -0.101)*
		Combined	(-0.175, -0.008)*
	Diastolic	Females	(-0.896, 0.523)
		Males	(-0.226, -0.026)*
		Combined	(-0.566, 0.186)
<i>ATP2B1</i>	Systolic	Females	(-0.284, 0.163)
		Males	(-0.184, 0.160)
		Combined	(-1.156, 0.121)
	Diastolic	Females	(-0.893, 0.104)
		Males	(-1.063, 0.352)
		Combined	(-2.279, 0.261)
<i>KCNK3</i>	Systolic	Females	(-0.195, 0.094)
		Males	(-0.195, -0.094)*
		Combined	(-0.161, 0.261)
	Diastolic	Females	(-0.353, 0.924)
		Males	(-0.186, -0.004)*
		Combined	(-1.287, 0.625)
<i>PRDM8</i>	Systolic	Females	(-0.750, 0.305)
		Males	(-0.214, -0.091)*
		Combined	(-0.253, -0.118)*
	Diastolic	Females	(-0.285, 0.361)
		Males	(-0.240, -0.024)*
		Combined	(-0.364, 0.028)

Table 4: Comparing empirical distributions of bootstrapped  $\hat{\sigma}_{CRIT} - \hat{\sigma}$  estimates.

## Appendix V: Data-splitting, cross-fitting inference, and estimation of $\hat{\sigma}_C^2$

Using Theorem 4 and Lemma 2, we get

$$\sqrt{n} \begin{pmatrix} \hat{H}(X) - H(X) \\ \hat{H}(Y) - H(Y) \end{pmatrix} \xrightarrow{\mathcal{D}} N(\mathbf{0}, \Sigma), \text{ as } n \rightarrow \infty,$$

where  $\Sigma$  is the  $2 \times 2$  dispersion matrix of  $(H_0(X), H_0(Y))'$ . Hence, we note that

$$\sqrt{n} \left( \hat{C}_{X \succ Y} - C_{X \succ Y} \right) \xrightarrow{\mathcal{D}} N(0, \sigma_C^2), \text{ as } n \rightarrow \infty.$$

Note that  $\sigma_C^2 := \sigma_{11} + \sigma_{22} - 2\sigma_{12}$ , where  $\sigma_{ij}$  is the  $(i, j)^{th}$  element of the covariance matrix given by  $\Sigma$ . To obtain  $\hat{\Sigma}$  we use the same data-splitting and cross-fitting technique described in Section 7.2 of the main article. For ease of exposition, we repeat the details of our estimation and inference technique below.

### Data-splitting

Let  $\mathcal{D} = \{(X_1, Y_1), \dots, (X_{2n}, Y_{2n})\}$  be a random sample drawn from a bivariate distribution  $f_{XY}$  with marginal  $f_X$  for  $X$  and  $f_Y$  for  $Y$ . Since we do not know  $f_X$  or  $f_Y$ , we invoke a data-splitting and cross-fitting technique to estimate the underlying density functions as well as the relevant entropy terms. That is, we first split the available data  $\mathcal{D}$  into two equal-sized but disjoint sets denoted by:

$$\mathcal{D}_1 := \{(X_1, Y_1), \dots, (X_n, Y_n)\} \text{ and } \mathcal{D}_2 := \{(X_{n+1}, Y_{n+1}), \dots, (X_{2n}, Y_{2n})\}.$$

Using one data split  $\mathcal{D}_1$ , we obtain estimates of the marginal density functions  $\hat{f}_{X;1}$  and  $\hat{f}_{Y;1}$  by the SCE method described in Section 7.1 of the main article. The estimated density functions are evaluated for data belonging to the second data split  $\mathcal{D}_2$  to obtain the following estimates of marginal entropies:

$$\widehat{H}_2(X) = -\frac{1}{n} \sum_{j=1}^n \ln \left( \hat{f}_{X;1}(X_{n+j}) \right), \text{ and } \widehat{H}_2(Y) = -\frac{1}{n} \sum_{j=1}^n \ln \left( \hat{f}_{Y;1}(Y_{n+j}) \right).$$

Interchanging the roles of data splits  $\mathcal{D}_1$  and  $\mathcal{D}_2$ , by a similar procedure, we obtain the estimated densities  $\hat{f}_{X;2}$  and  $\hat{f}_{Y;2}$ . The estimated density functions are evaluated for data belonging to data split  $\mathcal{D}_1$  to obtain the estimated entropies:

$$\widehat{H}_1(X) = -\frac{1}{n} \sum_{j=1}^n \ln \left( \hat{f}_{X;2}(X_j) \right), \text{ and } \widehat{H}_1(Y) = -\frac{1}{n} \sum_{j=1}^n \ln \left( \hat{f}_{Y;2}(Y_j) \right).$$

In anticipation of estimating the variance of  $\sqrt{n} \left( \hat{C}_{X \succ Y} - C_{X \succ Y} \right)$  later we define the following quantities:

$$\hat{\Sigma}(1) := \begin{Bmatrix} \hat{\sigma}_{11}(1) & \hat{\sigma}_{12}(1) \\ & \hat{\sigma}_{22}(1) \end{Bmatrix}, \quad \hat{\Sigma}(2) := \begin{Bmatrix} \hat{\sigma}_{11}(2) & \hat{\sigma}_{12}(2) \\ & \hat{\sigma}_{22}(2) \end{Bmatrix},$$

where the elements of  $\hat{\Sigma}(1)$  are given by:

$$\begin{aligned}\hat{\sigma}_{11}(1) &:= \frac{1}{n} \sum_{j=1}^n \left\{ -\log \left( \hat{f}_{X;2}(X_j) \right) - \hat{H}_1(X) \right\}^2, \\ \hat{\sigma}_{22}(1) &:= \frac{1}{n} \sum_{j=1}^n \left\{ -\log \left( \hat{f}_{Y;2}(Y_j) \right) - \hat{H}_1(Y) \right\}^2, \\ \hat{\sigma}_{12}(1) &:= \frac{1}{n} \sum_{j=1}^n \left\{ -\log \left( \hat{f}_{X;2}(X_j) \right) - \hat{H}_1(X) \right\} \times \left\{ -\log \left( \hat{f}_{Y;2}(Y_j) \right) - \hat{H}_1(Y) \right\}.\end{aligned}$$

Similarly, we define the elements of  $\hat{\Sigma}(2)$  as follows:

$$\begin{aligned}\hat{\sigma}_{11}(2) &:= \frac{1}{n} \sum_{j=1}^n \left\{ -\log \left( \hat{f}_{X;1}(X_{n+j}) \right) - \hat{H}_1(X) \right\}^2, \\ \hat{\sigma}_{22}(2) &:= \frac{1}{n} \sum_{j=1}^n \left\{ -\log \left( \hat{f}_{Y;1}(Y_{n+j}) \right) - \hat{H}_1(Y) \right\}^2, \\ \hat{\sigma}_{12}(2) &:= \frac{1}{n} \sum_{j=1}^n \left\{ -\log \left( \hat{f}_{X;1}(X_{n+j}) \right) - \hat{H}_1(X) \right\} \times \left\{ -\log \left( \hat{f}_{Y;1}(Y_{n+j}) \right) - \hat{H}_1(Y) \right\}.\end{aligned}$$

### Cross-fitting

Taking an average of the two sets of estimates, we obtain the so-called ‘‘cross-fitted’’ estimates of the marginal entropies:

$$\hat{H}(X) = \frac{\widehat{H}_1(X) + \widehat{H}_2(X)}{2}, \text{ and } \hat{H}(Y) = \frac{\widehat{H}_1(Y) + \widehat{H}_2(Y)}{2}.$$

Using these cross-fitted estimates we obtain  $\hat{C}_{X \succ Y} := \hat{H}(X) - \hat{H}(Y)$ . For variance estimation purposes, we will be using  $\hat{\Sigma} := (\hat{\Sigma}(1) + \hat{\Sigma}(2)) / 2$ .

### Inference

From Corollary 1 in the main article, we note that the asymptotic behaviour of  $\sqrt{n}\hat{C}_{X \succ Y}$  is given by

$$\sqrt{n} \left( \hat{C}_{X \succ Y} - C_{X \succ Y} \right) \xrightarrow{D} N(0, \sigma_C^2), \text{ as } n \rightarrow \infty,$$

where  $\sigma_C^2$  denotes the asymptotic variance of the estimate  $\hat{C}_{X \succ Y}$  and can be estimated using  $\hat{\Sigma}$  as follows:  $\hat{\sigma}_C^2 := \hat{\sigma}_{11} + \hat{\sigma}_{22} - 2\hat{\sigma}_{12}$ , where  $\hat{\sigma}_{ij}$  is the  $(i, j)^{th}$  element of the covariance matrix given by  $\hat{\Sigma}$ .

### References

P. M. Aronow and C. Samii. Estimating average causal effects under general interference, with application to a social network experiment. *Ann. of App. Stat.*, 11:1912–1947, 2017.



- A. R. Barron. Entropy and the central limit theorem. *Ann. of Prob.*, 14:336–342, 1986.
- A. Bernacchia and S. Pigolotti. Self-consistent method for density estimation. *J. Roy. Stat. Soc.: Series B*, 73:407–422, 2011.
- Patrick Blöbaum, Dominik Janzing, Takashi Washio, Shohei Shimizu, and Bernhard Schölkopf. Analysis of cause-effect inference by comparing regression errors. *PeerJ Computer Science*, 5:e169, January 2019. ISSN 2376-5992.
- C. Breunig and P. Burauel. Testability of reverse causality without exogeneous variation. 2021.
- S. Chatterjee. A new coefficient of correlation. *J. Amer. Stat. Assoc.*, 116:2009–2022, 2020.
- V. Chernozhukov, D. Chetverikov, M. Demirer, E. Duflo, C. Hansen, W. Newey, and J. Robins. Double/debiased machine learning for treatment and structural parameters. *The Econometrics Journal*, 21:1–68, 2018.
- J. Choi, R. Chapkin, and Y. Ni. Bayesian causal structural learning with zero-inflated poisson bayesian networks. In *Proc. of the 33rd Int. Conf. on Neur. Inf. Proc. Sys.*, pages 5887–5897, 2020.
- T. M. Cover. *Elements of Information Theory*. John Wiley & Sons, India, 2005.
- D. R. Cox. Role of models in statistical analysis. *Stat. Science*, 5:169–174, 1990.
- D. R. Cox. Causality: some statistical aspects. *J. Roy. Stat. Soc.: Series A*, 155:291–301, 1992.
- P. Daniušis, D. Janzing, J. Mooij, J. Zscheischler, B. Steudel, K. Zhang, and B. Schölkopf. Inferring deterministic causal relations. In *Proc. of the 26th Conf. on Uncertainty in AI*, page 143–150, 2010.
- D. A. Dicorpo, S. Lent, W. Guan, M. Hivert, and J S. Pankow. Mendelian randomization suggests causal influence of glycemic traits on DNA methylation. *Diabetes*, 67:1707, 2018.
- E. M. Domouzoglou, K. K. Naka, A. P. Vlahos, M. I. Papafaklis, L. K. Michalis, A. Tsatsoulis, and E. Maratos-Flier. Fibroblast growth factors in cardiovascular disease: The emerging role of fgf21. *Am. J. Physiol. Heart. Circ. Physiol.*, 309:1029–1038, 2015.
- R. Aylmer Fisher. *Stat. meth. for research workers*. Oliver and Boyd, Edinburgh and London, 6th edition, 1925.
- Josè A. R. Fonollosa. *Conditional Distribution Variability Measures for Causality Detection*, page 339–347. Springer International Publishing, 2019. ISBN 9783030218102.
- N. Friedman and I. Nachman. Gaussian process networks. In *Proc. of the 16th Conf. on Uncertainty in AI*, volume 16, pages 212–219, 2000.
- M. Gao and P. Ding. Causal inference in network experiments: regression-based analysis and design-based properties. *arXiv:2309.07476*, 2023.

- J. Hannig, H. Iyer, R. C. S. Lai, and T. C. M. Lee. Generalized fiducial inference: A review and new results. *J. Amer. Stat. Assoc.*, 111:1346–1361, 2016.
- M. Hernandez-Avila, T. Gonzalez-Cossio, E. Palazuelos, I. Romieu, A. Aro, E. Fishbein, K. E. Peterson, and H. Hu. Dietary and environmental determinants of blood and bone lead levels in lactating postpartum women living in Mexico City. *Env. Health Persp.*, 104:1076–1082, 1996.
- X. Hong, K. Miao, W. Cao, J. Lv, C. Yu, T. Huang, D. Sun, C. Liao, Y. Pang, Z. Pang, et al. Association between DNA methylation and blood pressure: a 5-year longitudinal twin study. *Hypertension*, 80:169–181, 2023.
- P. Hoyer, D. Janzing, J. M. Mooij, J. Peters, and B. Schölkopf. Nonlinear causal discovery with additive noise models. In *Proc. of the 21st Int. Conf. on Neur. Inf. Proc. Sys.*, page 689–696, 2008.
- G. W. Imbens and D. B. Rubin. *Causal Inference for Statistics, Social, and Biomedical Sciences: An Introduction*. Cambridge University Press, 2015.
- D. Janzing, J. Mooij, K. Zhang, J. Lemeire, J. Zscheischler, P. Danusis, B. Steudel, and B. Schölkopf. Information-geometric approach to inferring causal directions. *Artif. Int.*, 182:1–31, 2012.
- Diviyam Kalainathan, Olivier Goudet, and Ritik Dutta. Causal discovery toolbox: Uncovering causal relationships in python. *Journal of Machine Learning Research*, 21(37):1–5, 2020.
- M. P. Leung. Causal inference under approximate neighborhood interference. *Econometrica*, 90:267–293, 2022.
- C. F. Manski. Identification of treatment response with social interactions. *The Econometrics Journal*, 16:S1–S23, February 2013.
- J. M. Mooij, J. Peters, D. Janzing, J. Zscheischler, and B. Schölkopf. Distinguishing cause from effect using observational data: Methods and benchmarks. *J. Mach. Learn. Res.*, 17:1–102, 2016.
- Y. Ni. Bivariate causal discovery for categorical data via classification with optimal label permutation. In *Proc. of the 35th Int. Conf. on Neur. Inf. Proc. Sys.*, pages 10837–10848, 2022.
- T. A. O’Brien, K. Kashinath, N. R. Cavanaugh, W. D. Collins, and J. P. O’Brien. A fast and objective multidimensional kernel density estimation method: fastKDE. *Comp. Stat. & Data Anal.*, 101:148–160, 2016.
- Alon Orlitsky. Information theory. In *Encyclopedia of Physical Science and Technology*, pages 751–769. Elsevier, 2003.
- J. Pearl. *Causality: Models, reasoning and inference*. Cambridge University Press, England, 2009.

- S. Purkayastha and P. X.-K. Song. fastmi: A fast and consistent copula-based nonparametric estimator of mutual information. *J. Mult. Anal.*, page 105270, 2023.
- T. J. Rahman, B. M. Mayosi, D. Hall, P. J. Avery, P. M. Stewart, J. M. C. Connell, H. Watkins, and B. Keavney. Common variation at the 11- $\beta$  hydroxysteroid dehydrogenase type 1 gene is associated with left ventricular mass. *Circulation: Cardiovascular Genetics*, 4:156–162, 2011.
- D. B. Rubin. Estimating causal effects of treatments in randomized and nonrandomized studies. *J. Edu. Psych.*, 66:688, 1974.
- F. Sävje, P. Aronow, and M. Hudgens. Average treatment effects in the presence of unknown interference. *Ann. of Stat.*, 49:673, 2021.
- C. E. Shannon. A mathematical theory of communication. *Bell Sys. Tech. J.*, 27:379–423, 1948.
- P. X.-K. Song. *Correlated data analysis: Modeling, analytics, and applications*. Springer New York, NY, 2007.
- N. Tagasovska, V. Chavez-Demoulin, and T. Vatter. Distinguishing cause from effect using quantiles: Bivariate quantile causal discovery. In *Proc. of the 37th Int. Conf. on Mach. Lear.*, pages 9311–9323, 2020.
- R. Zamir. A proof of the fisher information inequality via a data processing argument. *IEEE Trans. on Info. Theo.*, 44:1246–1250, 1998.
- S. Zheng, N.-Z. Shi, and Z. Zhang. Generalized measures of correlation for asymmetry, nonlinearity, and beyond. *J. Amer. Stat. Assoc.*, 107:1239–1252, 2012.
- X. Zhou, Y. Jiao, J. Liu, and J. Huang. A deep generative approach to conditional sampling. *J. Amer. Stat. Assoc.*, 118:1837–1848, 2023.